An Executive Summary of the thesis entitled

"Synthesis, Spectral Characterization and Structural Analysis of Transition Metal Complexes Containing Acyl Pyrazolone Ligands and their Applications"

To be submitted to

The Maharaja Sayajirao University of Baroda

For the Degree of

DOCTOR OF PHILOSOPHY

In Chemistry

By

Barad Sapnaben Vishnubhai

Under the Guidance of

Dr. R. N. Jadeja

Department of Chemistry,

Faculty of Science,

The Maharaja Sayajirao University of Baroda

VADODARA- 390002,

GUJARAT

October 2024

Chapter 1

Introduction and literature review of transition metal complexes containing a derivative of pyrazolone ligands and their coordination chemistry

Chapter -**1** offers a brief overview of key advancements in transition metal chemistry, focusing on their coordination versatility, variable oxidation states and roles in catalysis, biology and materials science. It highlights significant discoveries in metal complexes' synthesis, characterization and applications, emphasizing their biological importance.

Transition metal chemistry and its characteristics

Transition metals are highly valued for their exceptional characteristics, making them superior in numerous applications compared to other elements. For instance, copper, a vital trace metal found in the form of Cu^{2+}, plays a significant role in metalloenzymes such as cytochrome oxidase, superoxide dismutase etc. While nickel is involved in the enzyme urease. Metal ions are essential in pharmaceuticals and are also used as diagnostic agents. The electronic configuration of Transition elements (3d elements) is characterized as, **3d elements (Z = 21 to 30): $[Ar]3d^{1\text{-}10}\,4s^2$**. Given the unique properties of metals, their advantages in drug discovery should be further harnessed for the design of new pharmaceuticals [1].

A pyrazolone chemistry

Pyrazolone can be viewed as a derivative of pyrazole possessing an additional carbonyl (C=O) group. Pyrazole (1H-pyrazole or 1,2-diazole) is a group of azole family, one of the most researched areas. Numerous applications in industries including technology, health and agriculture are made possible by various arrangements of the pyrazole nucleus [2][3]. These compounds feature a 5-membered heterocyclic structure with two adjacent nitrogen atoms with an additional carbonyl (C=O) group. Their first synthesis of 3-methyl-1-phenyl-5-pyrazolone was achieved by Ludwig Knorr in 1883 through a condensation reaction involving ethyl acetoacetate and phenylhydrazine [4].

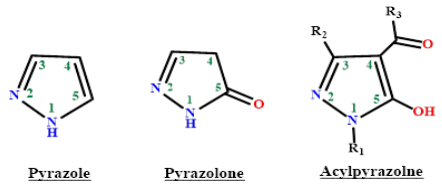

Fig.1.1. Structure of Pyrazole, Pyrazolone and Acypyrazolne

Acylpyrazolone and application

By 1959, Jensen and coworkers outlined a one-step synthesis method that involves acylating the C-4 position of the pyrazole ring in a basic dioxane solution with calcium

hydroxide at reflux temperature [5]. They are a class of β-diketones, where a pyrazole ring is integrated with a chelating functional group. Acylpyrazolone ligands have been used for complexation with various transition metals [6].

A brief review: Work done on Cu(II) and Ni(II) complexes

This section provides a brief literature review of both recent and past research on transition metal complexes with acylpyrazolones. The four, five and six coordinated copper complexes and six coordinated Ni(II) have been synthesized. The synthesized copper complexes exhibited biological activity. The recent reviews by Marchetti and colleagues have explored the various applications of pyrazolone-based transition metal complexes, as well as the properties and uses of acylpyrazolone ligands and their corresponding transition metal complexes [7][8]. Okafor has done some of the earliest publications on the Cu(II) complexes. Although Cu(II) complexes derived from pyrazolone derivatives are extensively researched for their biological effects [9]. The first known compound of Ni(II) 4-aminoalkylidene-5-pyrazolone was found to be dihydrate octahedral paramagnetic with two unpaired electrons [8].

***In vitro* Anticancer activity**

This section provides information about how the copper acylpyrazolone complexes are important as an anticancer agent having less side effects than cisplatin. MTT assay, live dead assay, scratch assay and gene expression study are the part of *in vitro* cytotoxicity assay. Cancer is characterized by uncontrolled cell proliferation, driven by transformed cells undergoing evolution through natural selection. MTT assay is a rapid colourimetric assay based on the tetrazolium salt MTT (3-(4,5-dimethylthiazol-2-yl)-2,5-diphenyl tetrazolium bromide), used to check the IC_{50} value of the compound against any cancer cell line. A promising method for investigating the behaviour of cancer cells is the scratch assay, which simulates wound healing to evaluate cell motility and proliferation. The Live/Dead assay is a common laboratory technique used in cell biology and toxicology to assess cell viability, distinguishing between live and dead cells within a population using specific dyes. Gene expression studies help understand the regulation of genes and their role in health, disease, and biological functions [10].

Aims and Objectives

The primary objective of this research is to synthesize acyl pyrazolone ligands and their complexes with copper and nickel transition metals. Comprehensive characterization was performed using techniques such as FTIR, NMR, TG-DTA, UV-VIS, Mass spectrometry, ESR and CV, along with single-crystal structure analysis. DFT and Hirshfeld studies were also conducted. Additionally, the *in vitro* anticancer activity of all the synthesized Cu(II) complexes has been assessed.

Chapter 2

Synthesis, Crystal Features and Characterization of a series of acylpyrazolone ligands: Computational analysis

Experimental work

Synthesis of ligands HL^{I} ,HL^{II} and HL^{III}

The synthetic pathway of HL^{I}, HL^{II} and HL^{III} ligands is depicted in **Fig.2.1** [5]. Furthermore, ligands HL^{IV}, HL^{V}, HL^{VI}, HL^{VII}, HL^{VIII} and HL^{IX} were synthesized using a similar method and have been reported previously by our lab [11,12,13,14].

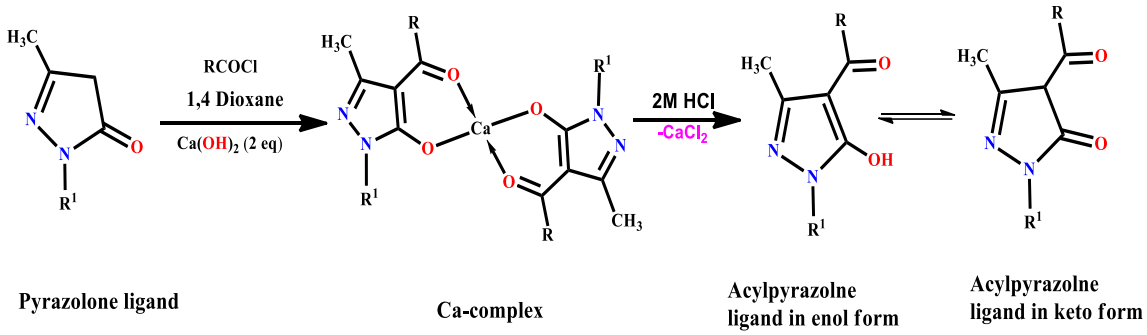

Fig.2.1. Synthetic route of ligands

> **R^{1}**= Phenyl, m-chloro phenyl and p-tolyl, **R**= 2,4-dichlorobenzoyl chloride (**HL^{I}, HL^{II} and HL^{III}**), **R**= 4-chlorobenzoyl chloride (**HL^{IV}, HL^{V} and HL^{VI}**), **R**= 3,5-dimethyl and 4-nitro benzoyl chloride (**HL^{VII}, HL^{VIII} and HL^{IX}**) ligands

HL^{I} ligand: Light creamish orange, **yield:** 85%, **M.P:** 128°C, **Molecular formula:** $C_{17}H_{12}Cl_2N_2O_2$, **M.W:** 347.20, **Elemental analysis**: C (Exp. 59.95%, Calc. 58.81%); H (Exp. 3.90%, Calc. 3.48%); N (Exp. 8.10%, Calc. 8.07%), **FTIR (KBr, cm^{-1}):** ν(C=O) of pyrazolone; (1627), ν(C=O) of 2,4 dichloro benzoyl; (1587), Cyclic ν(C=N); (1515), C–H in plane deformation; (1394), **NMR: ^{1}H NMR δ-ppm (400 MHz, $CDCl_3$):** 2.195 (s, 3H, CH_3(pyz)), 7.3–7.8 (m, Ar-H of HL^{I} ligand).

HL^{II} ligand: Light creamish orange, **yield:** 86%, **M.P:** 135°C, **Molecular formula:** $C_{17}H_{11}Cl_3N_2O_2$, **M.W:** 381.64, **Elemental analysis**: C (Exp. 54.10%, Calc. 53.50%); H (Exp. 3.05%, Calc. 2.91%); N (Exp. 7.50%, Calc. 7.34%), **FTIR (KBr, cm^{-1}):** ν(C=O) of pyrazolone; (1594), ν(C=O) of 2,4 dichloro benzoyl; (1550), Cyclic ν(C=N); (1482), C–H in-plane deformation; (1062), **^{1}H NMR δ-ppm (400 MHz, $CDCl_3$)**: d ppm:1.89 (s, 3H, Pyrazolone C-CH_3), 7.3–7.9 (m, Ar-H of HL^{II} ligand).

HL^{III} ligand: Orange-brown, yield: 86%, **M.P:** 135°C, **Molecular formula:** $C_{18}H_{14}Cl_2N_2O_2$, **M.W:** 361.22, **Elemental analysis**: C (Exp. 60.12%, Calc. 59.85%); H (Exp. 4.10%, Calc. 3.91%); N (Exp. 7.85%, Calc. 7.76%), **FTIR (KBr, cm^{-1}):** ν(C=O) of pyrazolone; (1668),

ν(C=O) of 2,4 dichloro benzoyl; (1585), Cyclic ν(C=N); (1472), C–H in-plane deformation; (1253), **^{1}H NMR δ-ppm (400 MHz, $CDCl_3$)**: d ppm:1.94 (s, 3H, Pyrazolone C-CH_3), 7.4–7.7 (m, Aromatic-H of HL^{III} ligand).

Results and discussion

^{1}H NMR and FTIR spectral studies

The ^{1}H NMR spectral analysis of HL^I, HL^{II}, and HL^{III} ligands was done in $CDCl_3$. The infrared spectra (4000-400 cm^{-1} KBr discs) of prepared ligands were done on model Brucker alpha.

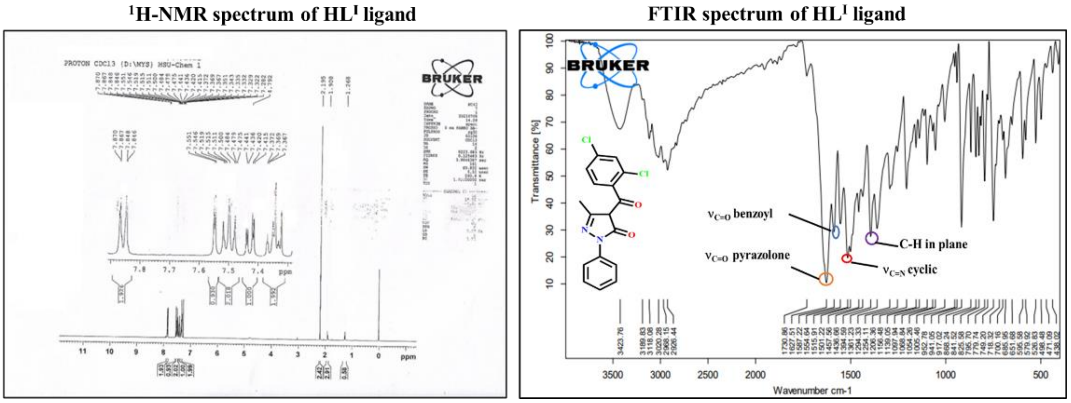

Fig.2.2. ^{1}H-NMR and FTIR spectra of ligand HL^I

Single crystal X-ray diffraction study

Crystal structure of HL^I, HL^{II}, and HL^{III} ligands was obtained in the form of keto, enol and keto having form '**Triclinic'** crystal system with ***P*-1** space group, '**Monoclinic'** crystal system with $P2_{1/n}$ space group**, 'Triclinic'** crystal system with ***P*-1** space group respectively.

DFT based computational analysis and Hirshfeld analysis

B3LYP/6-31G level basis set was used to compute the optimized geometry of ligands with energy values -49.934 keV, -62.440 keV and -51.004 keV for HL^I, HL^{II} and HL^{III} ligands accordingly. The distribution of frontier orbital can be used to analyse active sites and reactivity of complex. HOMO-LUMO gives an idea about the molecule's nature. To learn more about how molecules interact in crystal formations, we have employed Hirshfeld surfaces analysis. This study has provided a thorough description of the immediate surroundings of the molecule. The Crystal Explorer 17.5 programme was utilised to visualise and investigate intermolecular interactions and donor-acceptor interaction sites in this analysis. Energy calculations were carried out for a 3.8 Å cluster surrounding the chosen HS of ligands. The fast [HF/3-21G] model of the Crystal Explorer 17.5 program was utilised to calculate the interaction energy data [15].

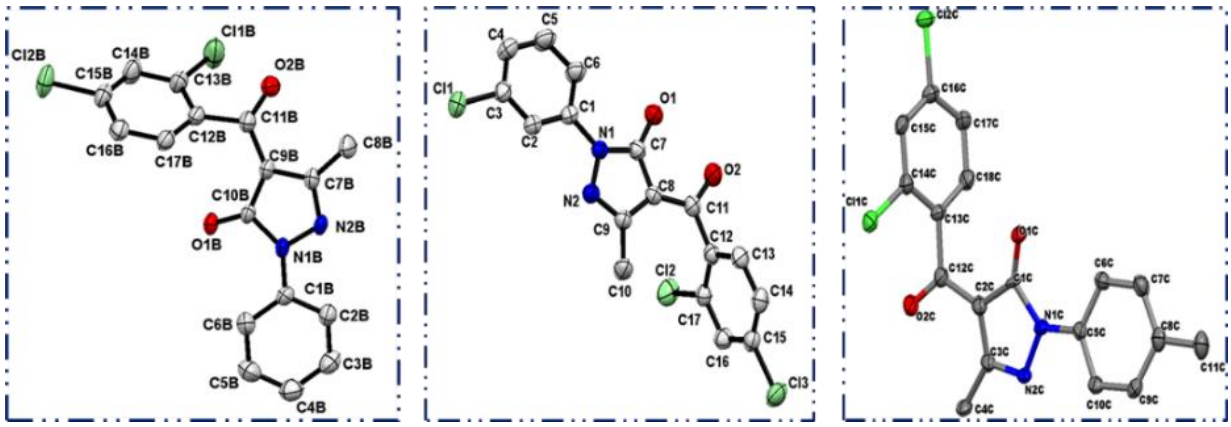

Fig.2.3. ORTEP diagram of HL^{I}, HL^{II}, HL^{III} ligands

Table 2.1. Crystal data and refinement parameters of ligands HL^{I}, HL^{II} and HL^{III}

Code	HL^{I} ligand	HL^{II} ligand	HL^{III} ligand
Unit cell dimension	a = 11.5502(3) Å b = 11.5976(3) Å c = 12.1851(3) Å	a = 7.44180(10) Å b = 11.3843(2) Å c= 19.8633(4) Å	a = 12.1180(3) Å b = 12.3703(4) Å c = 12.5275(5) Å
	α= 93.586(2)° β= 90.901(2)° γ= 105.568(2)°	α,γ = 90° β= 97.5520(10)°	α= 62.609(4)° β= 87.115(3)° γ= 87.752(3)°

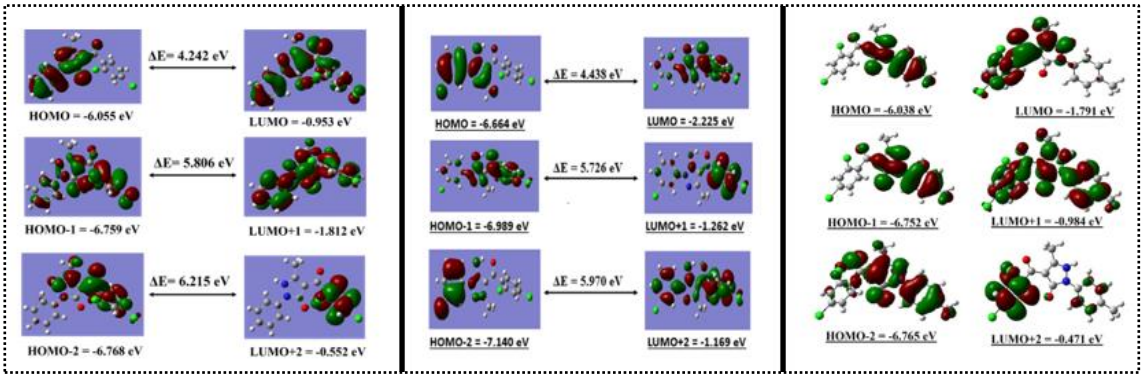

Fig.2.4. HOMO-LUMO molecular diagram of HL^{I}, HL^{II}, HL^{III} ligands

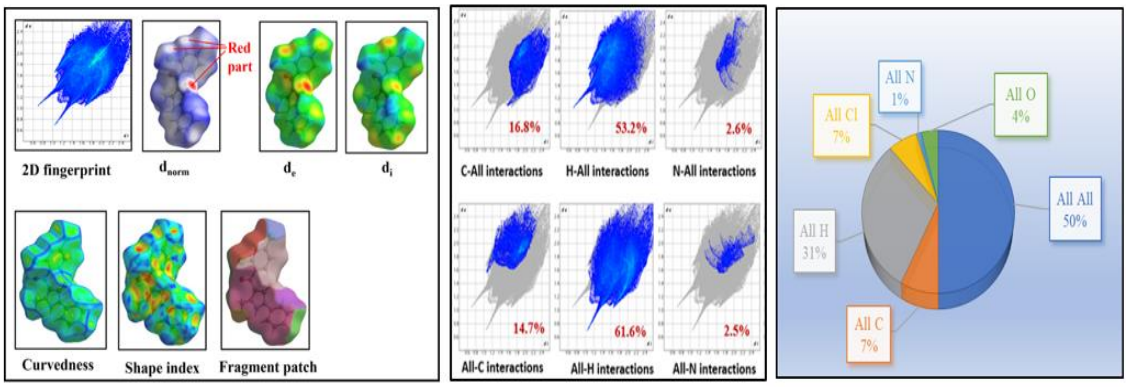

Fig.2.5. Hirshfeld diagram of HL^{I} ligand

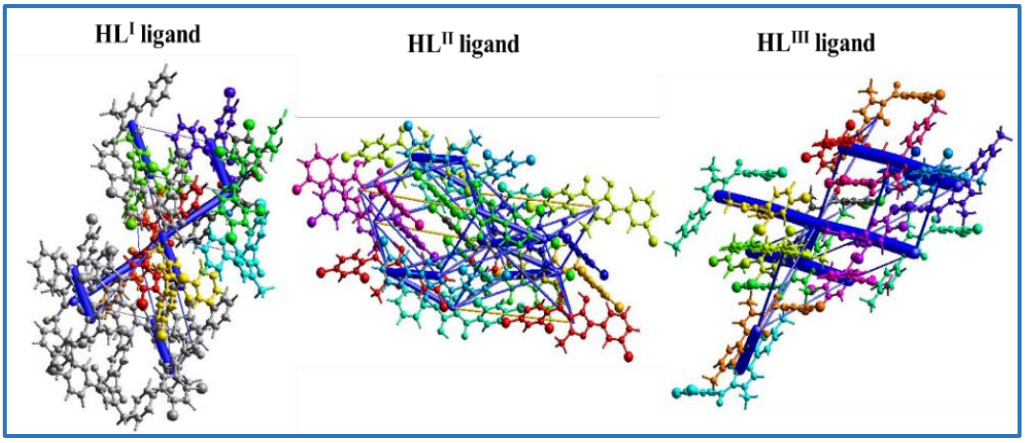

Fig.2.6. Energy frameworks of ligands based on Total energy

Conclusion

Three acylpyrazolone ligands were synthesized and characterized. Structural elucidation using FTIR spectral analysis shows significant vibrations. The single crystal data are largely used to examine their structure, geometry, composition, surface interactions, and lattice energy. The Hirshfeld surface analysis was also carried out to identify the crystal strength through interaction energies and intermolecular non-covalent surface interactions in the ligand.

CHAPTER 3

Synthesis, Characterization and Structural assessment of biologically active Square pyramidal Cu(II) acylpyrazolone complexes: DFT, Hirshfeld analysis

Part (a): Square pyramidal Cu(II) acylpyrazolone complex: Synthesis, characterization, crystal structure, DFT and Hirshfeld analysis, in-vitro anti-cancer evaluation

Experimental work

Synthetic route of complex-1 & complex-2

A hot methanolic solution of 1eq copper salt with 2 eq ligands HL^{II} and HL^{IX} was refluxed, yielding stable green plate-shaped crystals of complex-**1** and complex-**2** upon recrystallization in DMF and DMSO, respectively. Single-crystal X-ray analysis confirmed DMF and DMSO at the apical coordination site in each complex.

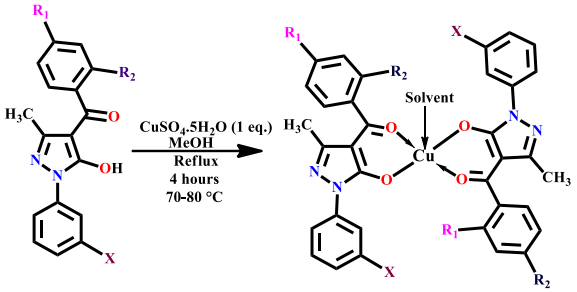

Complex-1: R_1= Cl, R_2= Cl, X= Cl, **Complex-2**: R_1= NO_2, R_2= H, X = H

Fig.3a.1. Synthetic route of complex-1 and complex-2

Complex-1: **Colour**: Green, yield: 82%, M.P:> 200°C, Molecular formula: $C_{34}H_{20}CuCl_6N_4O_4$.DMF, **M.W:** 824.811, **Elemental analysis**: C (Exp. 53.10%, Calc.: 52.69%); H (Exp. 2.90%, Calc. 2.80%); N (Exp. 8.21%, Calc. 7.21%); Cu (Exp. 8.10%, Calc. 7.08%), **Molar conductance (10^{-3} M DMF):** 2.18 $ohm^{-1}cm^2mol^{-1}$.

Complex-2: **Colour**: Green, yield: 83%, M.P.: >200°C, Molecular formula: $C_{34}H_{24}CuN_6O_8$.DMSO, **M.W:** 708.136, **Elemental analysis**: C (Exp. 56.55%, Calc. 55.53%); H (Exp. 4.50%, Calc. 4.03%); N (Exp. 10.80%, Calc. 10.50%); S (Exp. 2.80%, Calc. 2.77%); Cu (Exp. 8.05%, Calc. 7.94 %), **Molar conductance (10^{-3} M DMF):** 3.90 $ohm^{-1}cm^2mol^{-1}$.

Results and discussion

FTIR spectral studies

FTIR reveals critical information about the functional groups and molecular structures within the compound by analyzing how a sample absorbs infrared light. Theoretical vibrations can be

used to investigate the changes which occur during complexation. Theoretical IR frequencies were obtained using DFT calculations after the complete optimization.

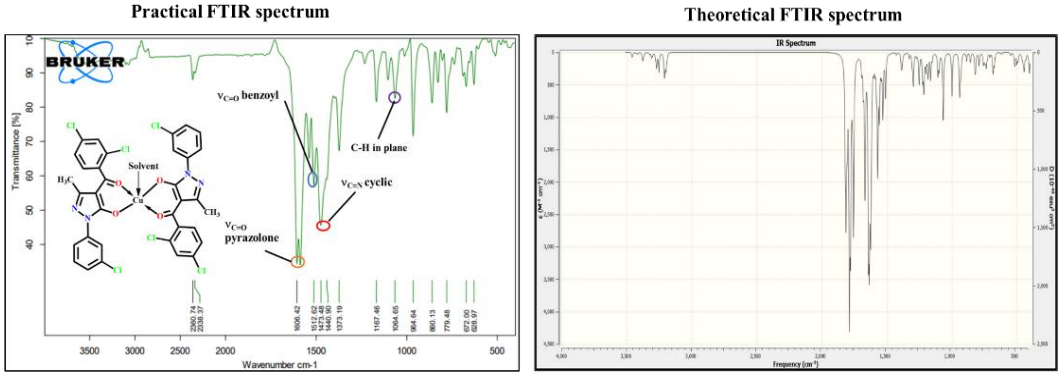

Fig.3a.2. FTIR spectra of complex-1

Table 3a.1. FTIR spectral data of ligands, complexes 1 and 2

Code	HL^{II} ligand	Complex-1	HL^{VI} ligand	Complex-2
ν(C=O) of benzoyl chloride	1550	1512	1519	1567
ν(C=O) of Pyrazolone	1594	1606	1622	1604
Cyclic ν(C=N)	1482	1473	1393	1380
C–H in plane deformation	1062	1064	1210	1244
ν_{M-O}	-	508	-	519

Thermogravimetric analysis

Three-step decomposition of 5 Co-ordinated complex-**1** can be examined through the TGA analysis. Degradation of both the ligands can be observed at the range of 280-500°C.

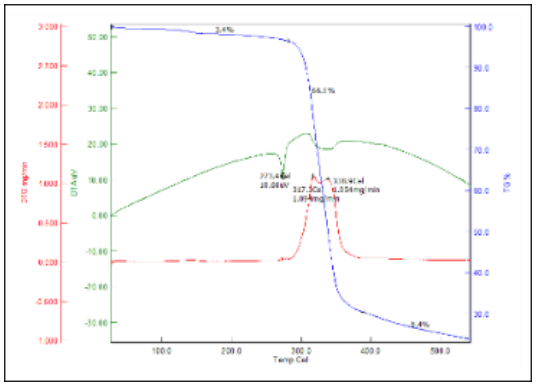

Fig.3a.3. TG-DTA plot of complex-1

Single crystal X-ray diffraction study

The green, thick plate-shaped crystals of both copper complexes have a square pyramidal geometry. Complex-**1** crystallizes in a triclinic system (***P*-1** space group with an inversion centre), while complex-**2** has a monoclinic system (***P*2$_{1/c}$** space group with a 2-fold screw axis and c-glide plane) [16].

Computational analysis employing DFT

The B3LYP/6-31G and LANL2DZ level basis sets were used to compute the optimized geometry with energy values -182.454 and -125.564 keV for complex-**1 and** complex-**2,**

respectively. Frontier orbitals have been studied because they are essential for determining chemical stability, energy value, and chemical behaviour.

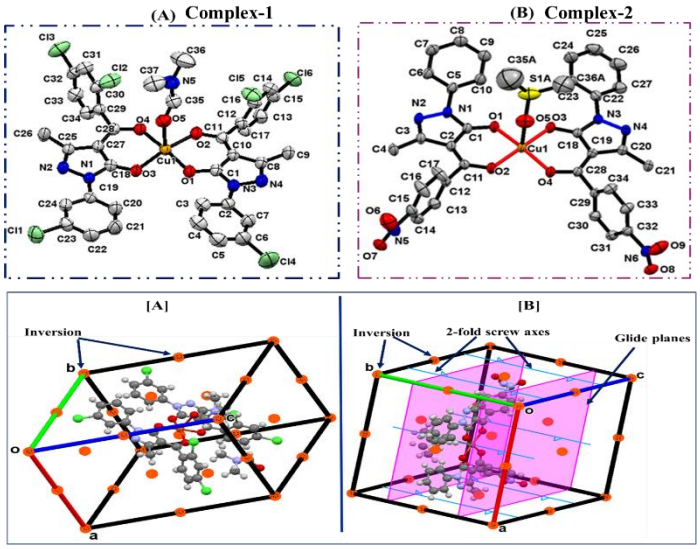

Fig.3a.4. ORTEP view and symmetry elements of [Cu(HL^{II})$_2$DMF] complex-1 and [Cu(HL^{IX})$_2$DMSO] complex-2

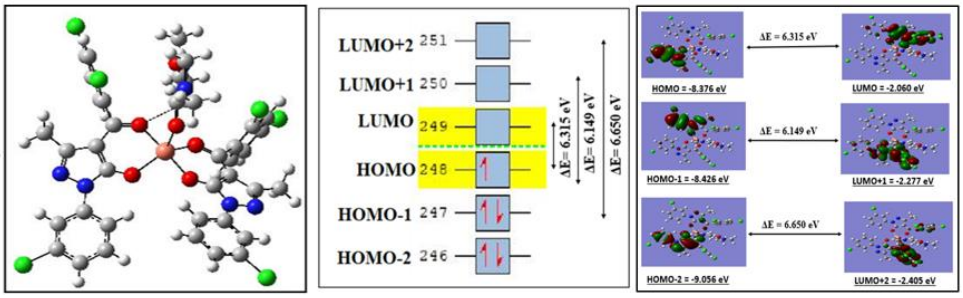

Fig.3a.5. DFT optimized structure and HOMO-LUMO orbital of complex-1

Table 3a.2. Global parameters of complex-1 and complex-2

Properties	Mathematical Formula	[Cu(HL^{II})$_2$DMF]	[Cu(HL^{IX})$_2$DMSO]
Ionization potential (IP)	IP = -E_{HOMO}	8.376	5.963
Chemical Potential (μ)	μ = 1/2 (E_{HOMO} + E_{LUMO})	-5.21	-4.501

Electronic spectral analysis and ESR analysis

UV-visible absorption spectra of both complexes were taken in DMSO solvent up to 950 nm. A complex-**1** exhibited a sharp transition at 277 nm whereas a complex-**2** exhibited n-π* transitions at 363 nm and π-π* transitions at 280 nm within the ultraviolet range due to intra-ligand charge transfer (ILCT) transitions. Additionally, the broad bands are observed at 800 nm and 768 nm in complex-**1** and complex-**2**, respectively. in the visible spectrum is attributed to a d-d transition. These transitions can be assigned to the $d_{x^2-y^2} \rightarrow d_{xz}$, d_{yz} and $d_{x^2-y^2} \rightarrow d_{z^2}$ transitions [17]. The ESR spectral analysis was carried out through ESR JEOL analysis in a Powder state at RT with tetracyanoethylene (TCNE) as a marker (g = 2.00277). Cu(II) exhibit

four lines which can be seen from the graph. In this analysis $g_{\parallel (2.361)} > g_{\perp (2.050)} > 2.0023$ which suggests the ground state results from dx^2-y^2 orbital.

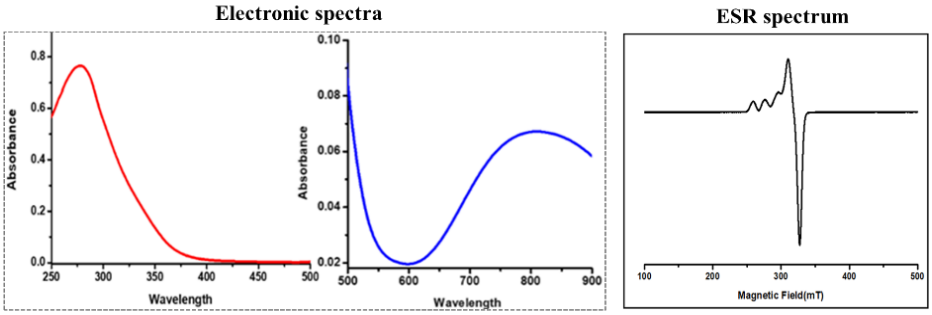

Fig.3a.6. Electronic spectra and ESR spectrum in powder form at RT of complex-1

Electro-chemical analysis (CV)

The redox behaviour of both complexes was studied through the cyclic voltammetry technique. value of ΔEp_1 is 0.5955 V and 0.3912 V for complex-**1** while, ΔEp_2 is 1.6433 V and 1.5650 V for complex-**2**, respectively for each redox couple. The nature of the graphs is quasi-reversible [18].

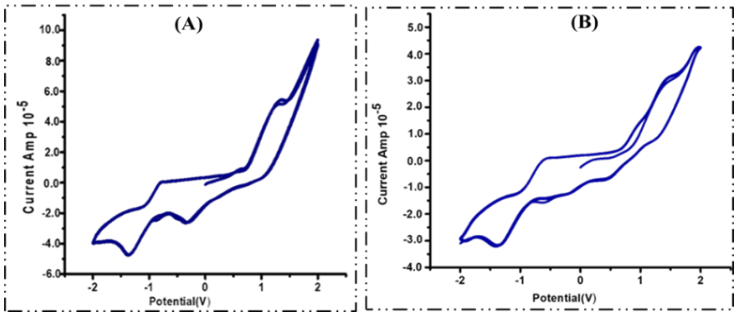

Fig.3a.7. Cyclic voltammograms of (A) complex-1 and (B) complex-2 in DMSO solution using 0.1 M TBAP at scan rate 100 mV and 50 mV, respectively

Hirshfeld surface analysis

This study has provided a thorough description of an immediate surroundings of the molecule. The Crystal Explorer 17.5 programme was utilised to visualise and investigate intermolecular interactions and donor-acceptor interaction sites in this analysis.

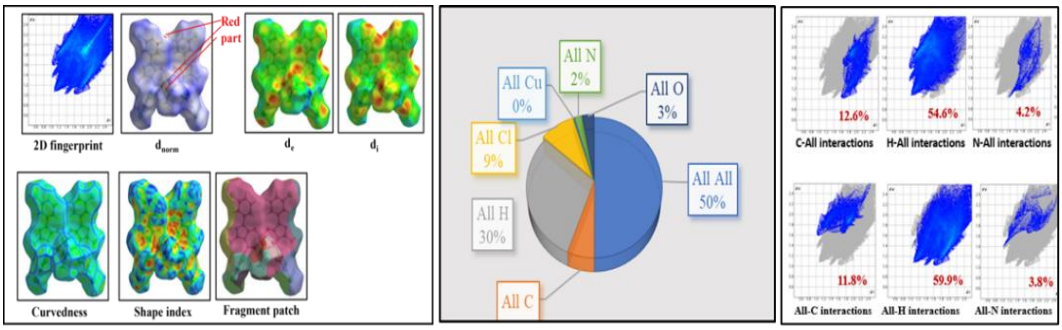

Fig.3a.8. Molecular Hirshfeld & 2d fingerprint plot of complex-1

In vitro Anticancer activity

The anticancer efficacy of both complexes was evaluated using a cytotoxicity assay, revealing a significant level of cytotoxic activity. Both complexes were tested against three different cancer cell lines: NCI-H23 (lung cancer), HepG2 (liver cancer) and SH-SY5Y

(neuroblastoma). **Table 3a.3. Percent inhibition (IC_{50} values) of complex-1 and complex-2 against NCI-H23, SH-SY5Y and HepG2 cancer cells**

Percent inhibition (IC_{50} values)			
Compounds	**Complex-1**	**Complex-2**	**Cisplatin**
NCI-H23	14.3 µM	-	17.65 µM
SH-SY5Y	7.2 µM	36.74 µM	44.94 µM
HepG2	7.1 µM	-	-

Cell death analysis & Scratch assay

Cell death analysis provides a count of live and dead cells using calcein and EthD-1 dyes responsible for green fluorescence (indicates live cells) and red fluorescence (indicates dead cells) respectively. Remarkable cell death could be observed as shown by predominant red fluorescence. Scratch assay is a straightforward and economical method to study cell migration in vitro. It has been examined at three different time intervals: at 0, 24 and 48 hrs. 41% and 29% wound closer were observed at 24 hrs in the treated condition.

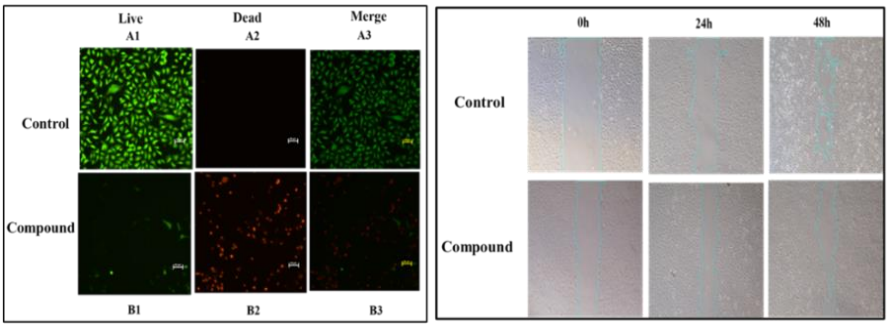

Fig.3a.9. (A) Dual staining (live/dead assay) of NCI-H23 cells exposed to complex-1, (B) Scratch assay

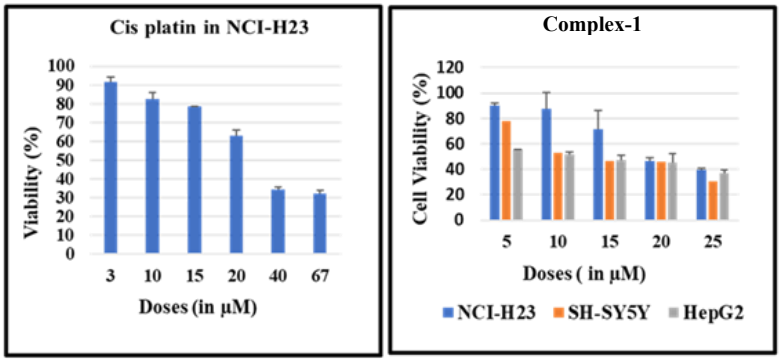

Fig.3a.10. Percent viability of NCI-H23 Cells exposed to indicated doses of Cisplatin and complex-1

Conclusion

This research highlights the pharmacological potential of pyrazolone-based Cu(II) complexes, complex-**1** and complex-**2,** synthesized and characterized through various analytical techniques. X-ray diffraction confirmed their square pyramidal geometry, with ligand oxygen atoms coordinating equatorially and DMF or DMSO axially. ESR and CV studies indicate paramagnetic and redox properties, while *in vitro* anticancer tests show promising results.

CHAPTER 3

Part (b): Acylpyrazolone based square pyramidal Cu(II) complexes: Synthesis, structural characterization, DFT and antiproliferative properties

Experimental work

Synthetic route of complex-3 & complex-4

Both copper complexes, complex-**3** and complex-**4**, were prepared using the same procedure described in Chapter **3a**

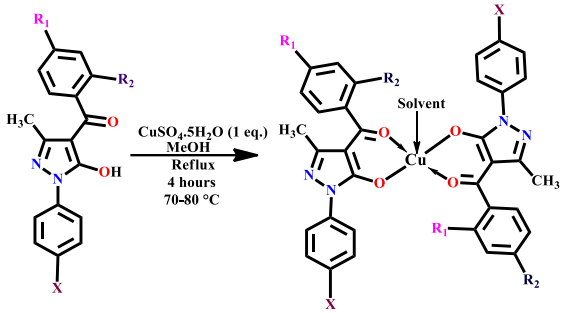

Fig.3b.1. Synthetic route of complex-3 and complex-4

Complex-3: Yellowish green, yield: 78%, M.P:> 200°C, Molecular formula: $C_{36}H_{26}CuCl_4N_4O_4$.DMF **Crystal:** Dark green prism-shaped, **M.W:** 783.974, **Elemental analysis**: C (Exp. 54.97%, Calc.: 54.65%); H (Exp. 3.98%, Calc. 3.88%); N (Exp. 8.90%, Calc. 8.71%); Cu (Exp. 8.00%, Calc.7.98 %), **FTIR (KBr, cm^{-1}):** ν(C=O) of pyrazolone: (1598), ν(C=O) of 2,4-dichloro benzoyl chloride: (1505), cyclic ν(C=N): (1363), **Molar conductance (10^{-3} M DMF):** 3.27 ohm^{-1}cm^{2}mol^{-1}.

Complex-4: Green, yield: 76%, M.P:> 200°C, Molecular formula: $C_{34}H_{24}CuCl_2N_4O_4$.DMSO, **Crystal:** Thick green plate-shaped, **M.W:** 687.031, **Elemental analysis**: C (Exp. 56.79%, Calc.: 56.51%); H (Exp. 4.10%, Calc. 3.95%); N (Exp. 7.56%, Calc. 7.32%); Cu (Exp. 8.04%, Calc. 8.01%), **Molar conductance (10^{-3} M DMF):** 3.87 ohm^{-1}cm^{2}mol^{-1}.

Results and discussion

FTIR spectral studies

FTIR is an instrumental technique which details the molecular properties of the synthesized copper complexes. During complexation, the charge from the O-atom of the C=O group in pyrazolone is transferred to the metal ion, which strengthens the M-O bond and weakens the C=O bond, leading to an increase in the bond length of the pyrazolone C=O bond [19]. Theoretical vibrations can be used to investigate the changes which occur during complexation. Theoretical IR frequencies were obtained using DFT calculations after the complete optimization.

Table 3b.1. FTIR spectral data of respective ligands, complexe-3 and complex-4

Code	HL^{III} ligand	Complex-3	HL^{IV} ligand	Complex-4
ν(C=O) of benzoyl chloride	1585	1505	1587	1575
ν(C=O) of Pyrazolone	1668	1598	1619	1597
Cyclic ν(C=N)	1472	1363	1557	1479
C–H in plane deformation	1253	1161	1213	1162
ν_{M-O}	-	508	-	490

Practical FTIR spectrum complex-3 | Theoretical FTIR spectrum complex-3

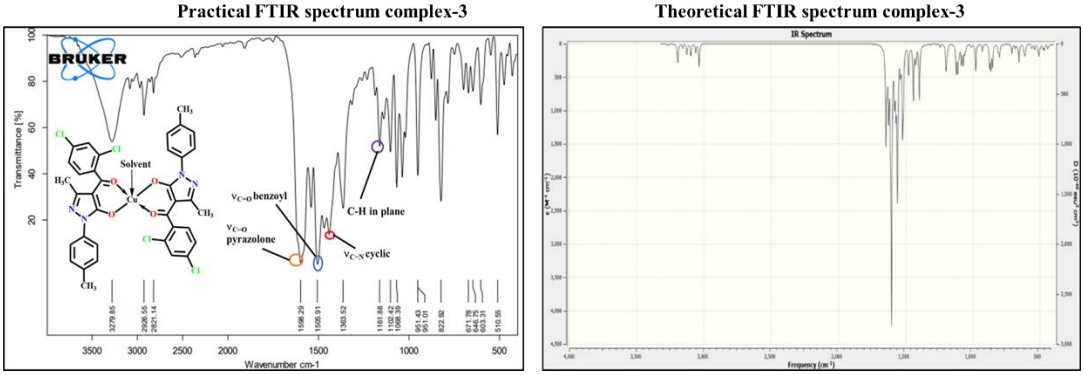

Fig.3b.2. FTIR spectra of complex-3

Thermogravimetric analysis

TGA analysis, explains how a material's mass changes with temperature. The aforementioned methodology can be used to evaluate 3 steps decomposition of complex-**3** and complex-**4.**

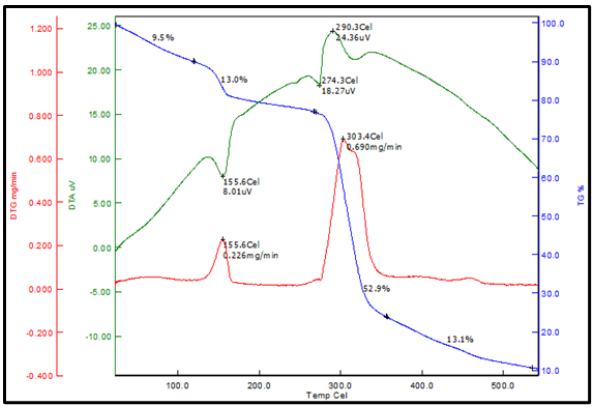

Fig.3b.3. TG-DTA plot of complex-3

Single crystal X-ray diffraction study

The complex-**3** and complex-**4** were recrystallized in DMF and DMSO solvents, respectively. Thick green crystals of both complexes were obtained. The geometry of the synthesized complexes was determined to be square pyramidal (penta-coordinated), where four oxygen atoms from two ligands occupy the equatorial positions and the fifth position is coordinated by an oxygen atom from a DMF molecule (in complex-**3**) and a DMSO molecule (in complex-**4**).

DFT-based computational analysis

The geometries of complexes **3** and **4** were computed at B3LYP/LANL2DZ and B3LYP/6-31G levels, yielding optimization energies of -65.6225 keV and -60.4222 keV (B3LYP/LANL2DZ)

and -139.7153 keV and -134.5150 keV (B3LYP/6-31G) for complexes **3** and **4,** respectively. HOMO-LUMO energies are vital for understanding various chemical interactions.

Table 3b.2. Refinement parameters of complex-3 and complex-4

CODE	$[Cu(HL^{III})_2DMF]$ Complex-3	$[Cu(HL^{IV})_2DMSO]$ Complex-4
Crystal system	Monoclinic	Monoclinic
Space group	$P2_1/n$	$P2_1/c$
Unit cell dimension	a= 13.9750(17) Å b= 6.8795(9) Å c= 39.669(5) Å	a= 14.415(4) Å b= 16.478(4) Å c= 14.620(4) Å
	α,γ = 90° β=93.355(6)°	α,γ = 90° β= 101.557(8)°

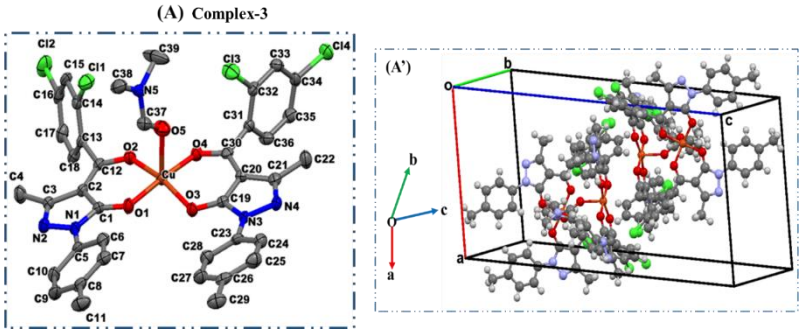

Fig.3b.4. ORTEP view and crystal packing of $[Cu(HL^{III})_2DMF]$ complex-3

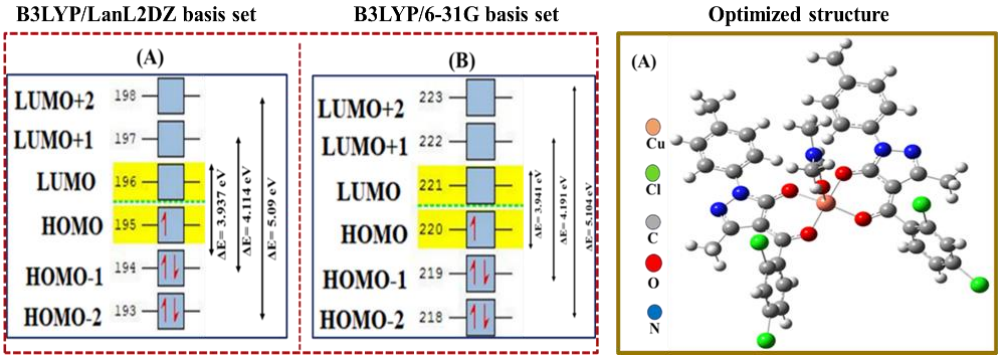

Fig.3b.5. HOMO-LUMO energy diagram and DFT optimized structure of complex-3

Table 3b.3. Global parameters (at LanL2DZbasis set) of complex-3 and complex-4

Properties	Mathematical Formula	$[Cu(HL^{III})_2DMF]$	$[Cu(HL^{IV})_2DMSO]$
Ionization potential (IP)	$IP = -E_{HOMO}$	5.794	5.950
Chemical Potential (μ)	$\mu = 1/2 (E_{HOMO} + E_{LUMO})$	-3.825	-4.027

Electronic spectral analysis, ESR analysis

UV-visible absorption analysis of the copper complexes in DMSO, up to 950 nm, identified an energy gap with transitions ($d_{x^2-y^2} \rightarrow d_{xz}$, d_{yz}, and $d_{x^2-y^2} \rightarrow d_{z^2}$) linked to Jahn-Teller distortion, specifically the $^2E_g \rightarrow {}^2T_{2g}$ transition, confirming a square pyramidal geometry for both complexes [20].

Complex-3: d-d transition (751 nm), Molar absorbance (ε): 57.1 M^{-1} cm^{-1}

Complex-4: d-d transition (768 nm) Molar absorbance (ε): 89.1 M^{-1} cm^{-1}

To explain the magnetic behaviour of the copper complexes ESR analysis was conducted. Tetracyanoethylene (TCNE) was used as a marker (g = 2.00277) during the ESR JEOL analysis in the powder state at RT at in the solution state at LNT. The graphs show four lines that represent Cu(II). The value of $g_{||}$ at RT is 2.545 and at LNT is found to be 2.353 for complex-**3.**

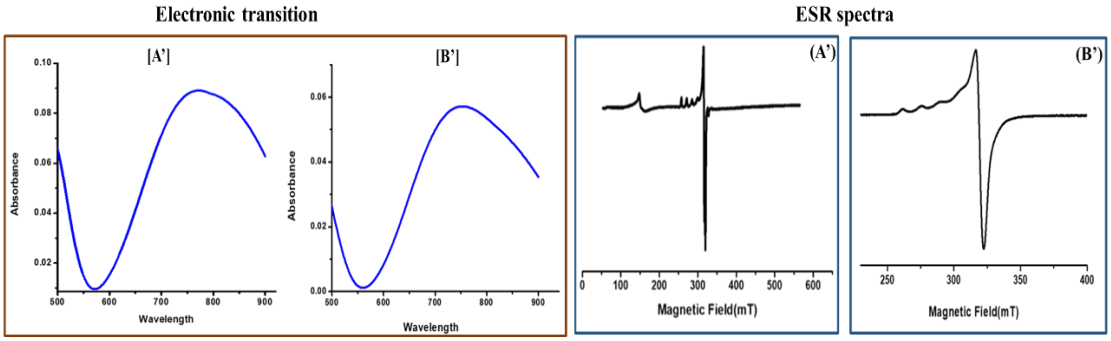

Fig.3b.6. Electronic spectra and ESR spectra in solution stat at LNT of (A') complex-3 & (B') complex-4

Hirshfeld surface area analysis &2d fingerprint plots

Hirshfeld surface analysis and 2D fingerprint plots were generated using CrystalExplorer17.5 to examine structural relationships and interactions, including hydrogen bonding, in these related compounds. Key surface features analyzed include normalized distance (dnorm), de, di, shape index, curvedness, and fragment patch.

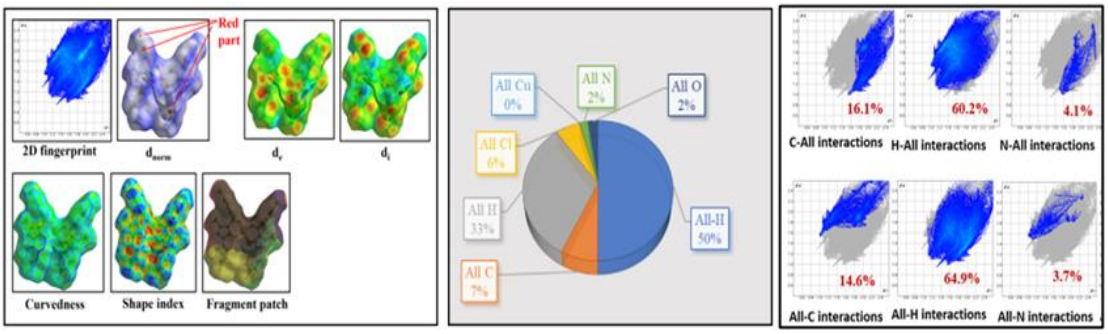

Fig.3b.7. Molecular Hirshfeld & 2d fingerprint plots of complex-3

Cytotoxicity assay

In vitro, anticancer activity of a complex-2 has been done against NCI-H23, SH-SY5Y and HepG2 cells. Complex-**3** was assessed against SH-SY5Y cancer cells since this complex shows greater effectivity against the SH-SY5Y cell line hence we are reporting the IC_{50} value of this complex on neuroblastoma cancer cells which is 10.8 µM. A comparative study with cisplatin is also reported.

Table 3b.4. Percent inhibition (IC_{50} values) of complex-3 and complex-4 against NCI-H23, SH-SY5Y and HepG2 Cells

Percent inhibition (IC_{50} values)			
Compounds	**Complex-3**	**Complex-4**	**Cisplatin**
NCI-H23	4.8 µM	-	17.65 µM
SH-SY5Y	11.41 µM	10.8 µM	44.94 µM
HepG2	11.07 µM	-	-

3b.2.8.1. Cell death analysis & Scratch assay

Cell death analysis with calcein and EthD-1 dyes showed green fluorescence for live cells and red for dead cells, demonstrating complex-3's higher efficacy against NCI-H23 cells. In the scratch assay, used to assess cell migration, complex-**3** treatment resulted in 26% wound closure at 24 h and 75% at 48 h, significantly inhibiting the migratory ability of NCI-H23 lung cancer cells compared to controls [21,22].

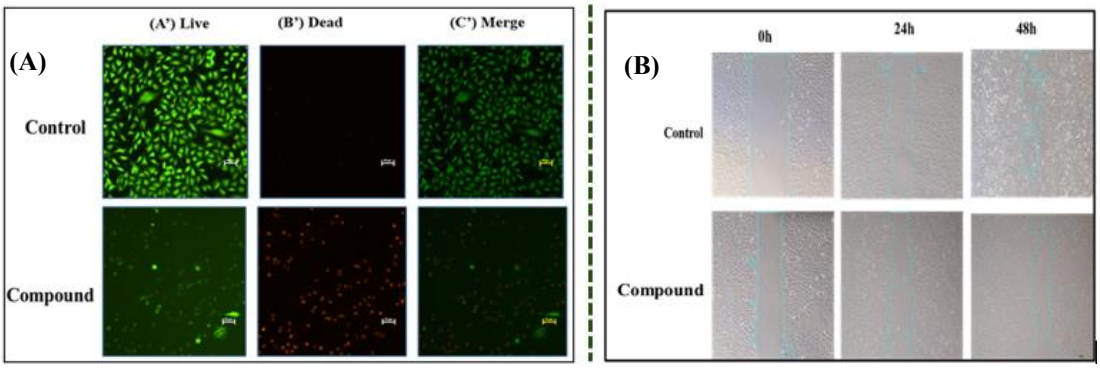

Fig.3b.8. (A) Dual staining (live/dead assay) of NCI-H23 cells exposed to complex-3, (B) Scratch assay

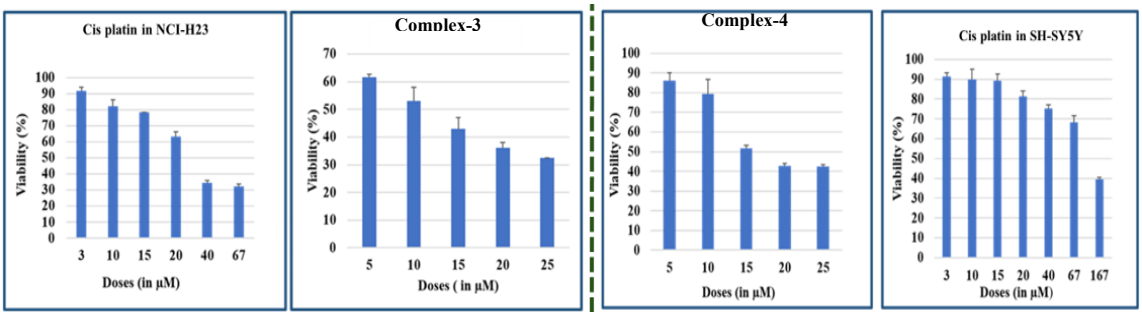

Fig.3b.9. (i)Percent viability of NCI-H23 Cells exposed to indicated doses of Cisplatin & complex-2
(ii) Percent viability of NCI-H23 Cells exposed to indicated doses of Cisplatin and complex-3

Conclusion

The design and synthesis of pyrazoles is a promising topic of research since they are an important pharmacophore with a diversity of biological characteristics. In this research we discussed the synthesis and characterization of complex-**3** & complex-**4**. Square Pyramidal geometry of the stable copper complexes demonstrated by single crystal X-ray crystallography. B3LYP/6-31G and B3LYP/LANL2DZ two different basis set were used to optimized both complexes. *In vitro* anticancer activity indicates the positive application of the complex. We found that lung cancer cells' ability to survive and spread can be inhibited by the complex-**3**.

CHAPTER 4

Synthesis of New Square planar Cu(II) complexes derived from acylpyrazolone ligand: Molecular structure Computational, Hirshfeld analysis and antiproliferative properties

Part (a): Cytotoxicity assay and gene expression studies of acylpyrazolone-based square planar Cu(II) complexes: synthesis, characterization and computations

Experimental work

Synthetic route of complex-5 & complex-6

Both copper complexes, complex-**5** and complex-**6**, were prepared using the same procedure outlined in Chapter **3a.**

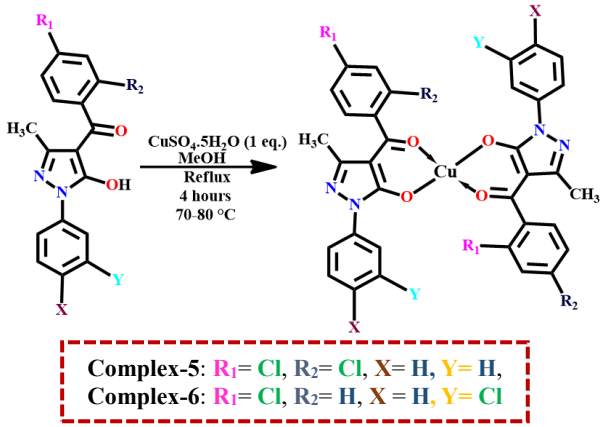

Fig.4a.1. Synthetic route of complex-5 and complex-6

Complex-5: Green colour, yield: 85%, M.P:> 200°C, Molecular formula: $C_{34}H_{22}Cl_4CuN_4O_4$, M.W: 755.921, Elemental analysis: C (Exp. 53.92%, Calc. 54.02%); H (Exp. 2.90%, Calc. 2.93%); N (Exp. 6.96%, Calc. 7.41%); Cu (Exp. 8.10%, Calc. 8.08%), **FTIR (KBr, cm^{-1}):** ν(C=O) of pyrazolone: (1602), ν(C=O) of 2,4-dichloro benzoyl chloride: (1577), cyclic ν(C=N): (1435).

Complex-6: Greenish yellow colour, yield: 86%, M.P:> 200°C, Molecular formula: $C_{38}H_{36}Cl_2N_5NiO_6$, M.W: 788.32, gravimetrically and volumetrically, Elemental analysis: C (Exp. 49.20%, Calc. 49.49%); H (Exp. 3.03%, Calc. 3.03%); N (Exp. 7.50%, Calc. 7.80%); Cu (Exp. 8.07%, Calc. 8.05%), (Metal estimation- gravimetrically and volumetrically), ν(C=O) of pyrazolone: (1601), ν(C=O) of 2,4-dichloro benzoyl chloride: (1586), cyclic ν(C=N): (1475).

Results and discussion

FTIR spectral and Thermogravimetric analysis

The copper complexes thermally decompose between 100 and 550°C, demonstrating remarkable thermal stability. Degradation of ligand moiety is 76.5% and 63.5% in complex-**5** and complex-**6** respectively.

Table 4a.1. FTIR spectral data of respective ligands, complexe-5 and complex-6

Code	HL^{I} ligand	Complex-5	HL^{V} ligand	Complex-6
ν(C=O) of benzoyl chloride	1587	1577	1590	1586
ν(C=O) of Pyrazolone	1627	1602	1625	1601
Cyclic ν(C=N)	1515	1435	1551	1475
C–H in plane deformation	1394	1379	1385	1360
ν_{M-O}	-	508	-	490

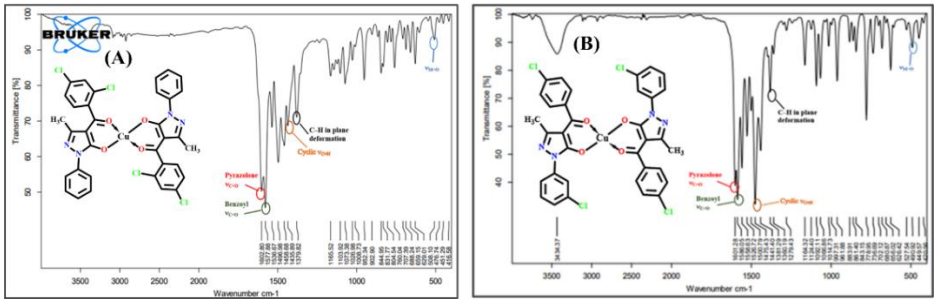

Fig.4a.2. FTIR spectra of (A) complex-5 & (B) complex-6

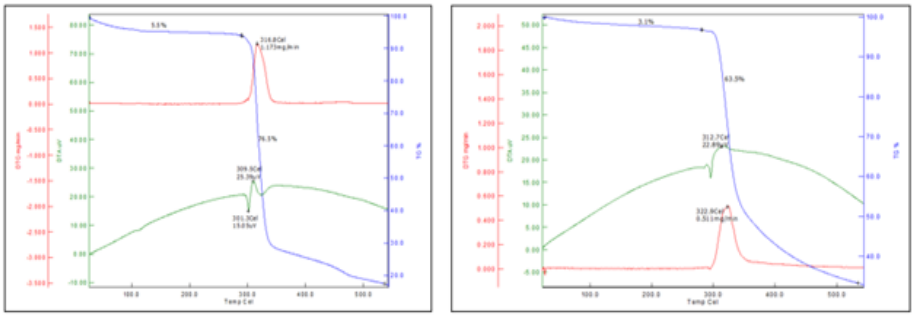

Fig.4a.3. TG-DTA plot of complex-5 & complex-6

Single crystal X-ray diffraction study

$[Cu(HL^{I})_2]$ complex-5: α= 90.834(4)°, β= 95.017(4)°, γ=106.124(4)°, a = 9.6075(12)Å, b= 11.7452(15)Å, c= 14.3696(17)Å, Triclinic space group *P*-1.

$[Cu(HL^{V})_2]$ complex-6: α= 90°, β= 111.660(4)°, γ=90°, a = 9.0930(11)Å, b= 27.412(3)Å, c= 6.8238(8)Å, Monoclinic space group $P2_1/c$.

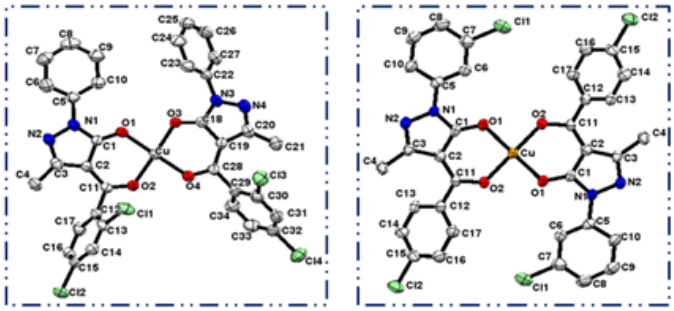

Fig.4a.4. ORTEP view of $[Cu(HL^{I})_2]$ complex-5 & $[Cu(HL^{V})_2]$ complex-6

DFT-based computational analysis & Hirshfeld surface area analysis

The geometry optimization of complex-**5** and complex-**6** was done via B3LYP/6-31G level basis set using Gauss View 6.0 software. The energy values of complex-**5** and complex-**6** are -144.475 keV, -144.475 keV. HOMO-LUMO energies play an essential role in determining a variety of chemical interactions.

With the help of Crystal Explorer 17.5 program, the donor-acceptor interaction sites and intermolecular contacts can be visualized in this analysis 3D Hirshfeld surfaces have been mapped over dnorm, de, di, shape index, curvedness and fragment patch.

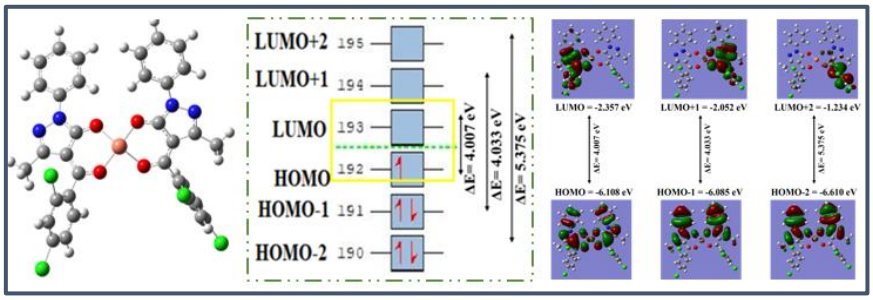

Fig.4a.5. DFT optimized geometry & HOMO-LUMO orbital of complex-5

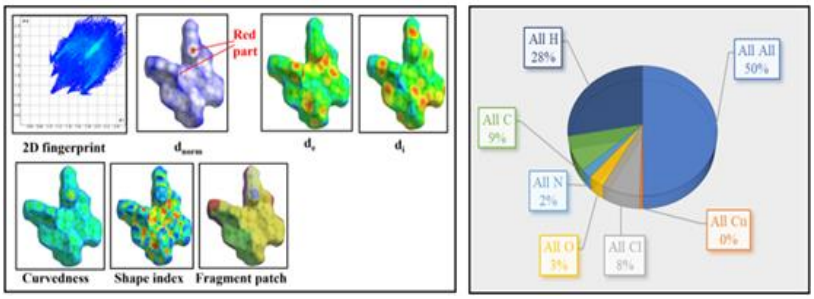

Fig.4a.6. Molecular hirshfeld diagram of complex-5

Electronic spectral analysis

The electronic spectra of square planar complex-**5** and complex-**6** were recorded in a DMSO. The crystal sample underwent UV-visible absorption investigations up to 950 nm to determine the energy gap of copper complexes. DMSO solvent was used for the analysis. The particular transition occurs from the $^2E_g \rightarrow {}^2T_{2g}$ transition.

Complex-5: π-π*(277 nm), n-π*(333 nm), d-d transition (742 nm)

Complex-6: π-π*(283 nm), n-π*(352 nm), d-d transition (739 nm)

ESR & Electrochemical analysis

The ESR spectral analysis of two copper complexes was carried out using ESR JEOL analysis in the powder state at RT and the solution state at LNT. The value of $g_{\|}$ for complex-**5** and complex-**6** is found to be 2.370 (RT), 2.370 (LNT) and 2.204 (RT), 2.313 (LNT), respectively, and the value for $g_{\perp}$ is found to be 2.063, 2.052 for complex-**5** and complex-**6,** respectively. The g tensor values, where $g_{\|} > g_{\perp} > 2.0023$ indicate the presence of an unpaired electron in a dx^2-y^2 orbital. The redox behaviour of both complexes was studied through the cyclic voltammetry (CV) technique. The ratio of the first anodic to cathodic peak current (Ipa_1/Ipc_1) for complex-**5** is -0.0046 amp and for the second peak (Ipa_2/Ipc_2) is -2.4671 amp. For complex-**6**, the (Ipa_1/Ipc_1) ratio is -0.0047 amp and (Ipa_2/Ipc_2) ratio is -2.1788 amp.

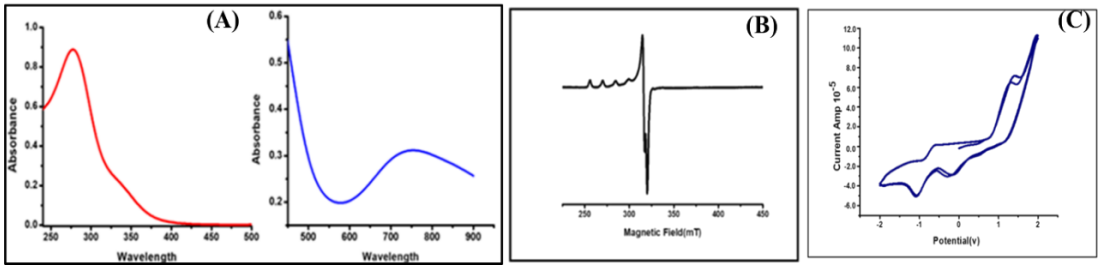

Fig.4a.7. Complex-5: (A) Electronic spectra, (B) ESR spectrum at LNT, (C) CV plot

Cytotoxicity assay

Cell viability was assessed using an MTT assay. The copper complexes were able to inhibit the cell viability of NCI-H23, SH-SY5Y and HepG2 cancer cells. IC_{50} was calculated against Cisplatin on the SH-SY5Y neuroblastoma cancer cell line. The IC_{50} value is 44.94µM for cisplatin. Complex-**5** gave the best result against the SH-SY5Y cell line. Hence further study has been done on a complex-**5**. Such as Live/dead assay and Gene expression study by qRT-PCR against BAD and BCL2L1 genes. The IC_{50} value for complex-**5** is 7.2 µM, 12.3 µM, and 9.0 µM and complex-**6** was reported to be 8.4 µM, 8.4 µM, and 10.7 µM against NCI-H23, SH-SY5Y and HepG2 cells respectively.

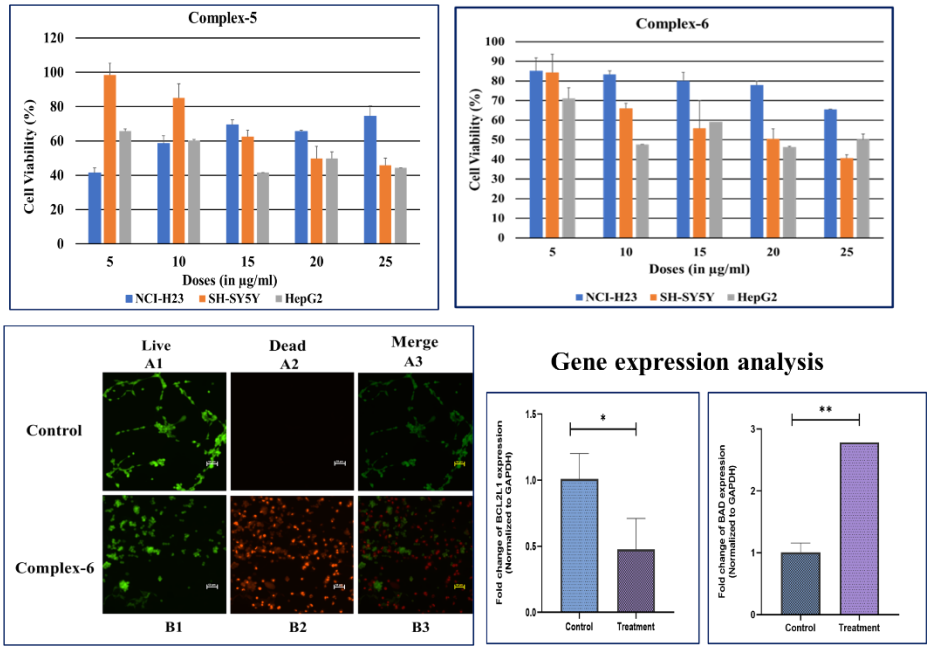

Fig.4a.8. Percent cell viability of NCI-H23, SH-SY5Y and HepG2 cells exposed to indicated doses of complex-5 and 6, Live/dead assay of SH-SY5Y cells exposed to complex-6, Gene expression analysis of complex-6

Conclusions

Two acyl pyrazolone-based Cu(II) complexes were synthesized and characterized, with X-ray crystallography confirming a square planar geometry. DFT/B3LYP/6-31G optimization and ESR studies revealed paramagnetic behaviour. Hirshfeld surface analysis examined intermolecular interactions, while in vitro anticancer tests showed promising applications.

CHAPTER 4

Part (b): Two New Square Planar Cu(II) complexes derived from a heterocyclic Pyrazolone ligand: Synthesis, *in vitro* anticancer activity, DFT and Hirshfeld analysis

Experimental work

Synthetic route of complex-7 & complex-8

Both copper complexes, complex-**7** and complex-**8**, were prepared using the same procedure outlined in the above chapters.

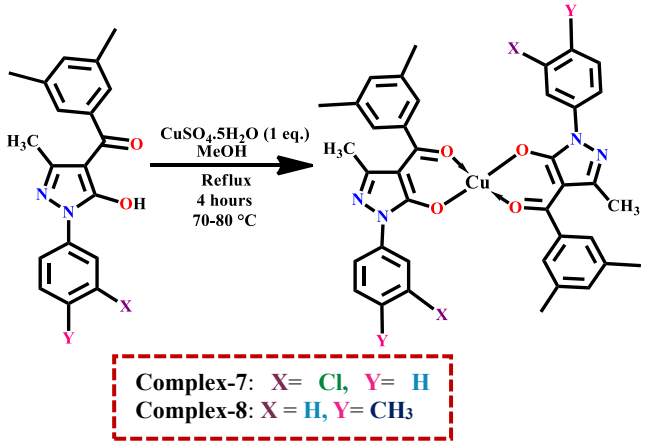

Fig.4b.1. Synthetic route of complex-7 and complex-8

Complex-7: Green, yield: 82%, M.P:> 200°C, Molecular formula: $C_{38}H_{32}CuCl_2N_4O_4$, **Crystal:** Pale green-yellow thick needle, M.W: 743.14, **Elemental analysis**: C (Exp. 60.97%, Calc.: 61.42%); H (Exp. 4.86%, Calc. 4.34%); N (Exp. 8.23%, Calc. 7.54%); Cu (Exp. 8.30%, Calc. 8.55%), **FTIR(KBr, cm^{-1}):** 1585 ($\nu_{C=O}$ of pyrazolone), 1603 ($\nu_{C=O}$ of 3,5-dimethyl benzoyl), 1485 ($\nu_{C=N}$), 596 (ν_{Cu-O}), **Molar conductance(10^{-3} M DMF):** 4.0 ohm^{-1}cm^{2}mol^{-1}.

Complex-8: Yellowish green, yield: 80 %, M.P: >200°C, Molecular formula: $C_{40}H_{38}CuN_4O_4$, **Crystal:** thick plates M.W: 702.30, **Elemental analysis**: C (Exp. 67.95%, Calc.: 68.41%); H (Exp. 4.98%, Calc. 5.45%); N (Exp. 6.90%, Calc. 7.98%); Cu (Exp. 8.80%, Calc. 9.05%), **FTIR(KBr, cm^{-1}):** 1526 ($\nu_{C=O}$ of pyrazolone), 1593 ($\nu_{C=O}$ of benzoyl), 1492 ($\nu_{C=N}$), 513 (ν_{Cu-O}), **Molar conductance(10^{-3} M DMF):** 4.5 ohm^{-1}cm^{2}mol^{-1}.

Results and discussion

FTIR and Thermogravimetric analysis

The mass loss and thermal stability of the material are inferred via thermogravimetric analysis (TGA). Thermal breakdown of the copper at temperatures around 100 and 550 °C demonstrates the remarkable thermal stability of both complexes. TGA analysis of complex-**7** & complex-**8** revealed a total weight loss of 61.8% and 49.64% on the TG graph respectively.

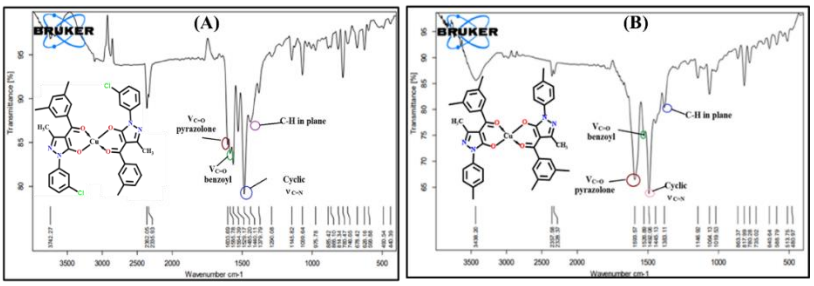

Fig.4b.2. FTIR spectra of (A) complex-7 & (B) complex-8

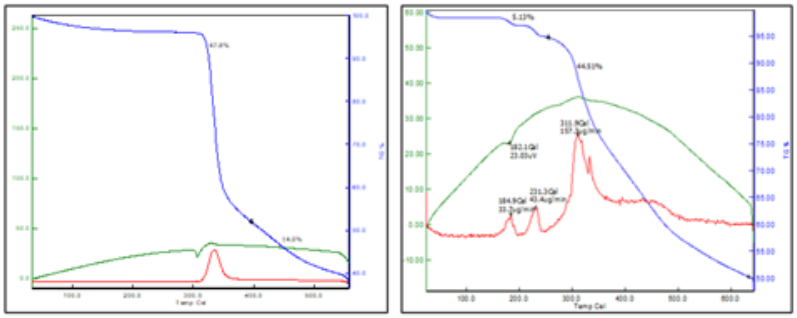

Fig.4b.3. TG-DTA plot of complex-6 & complex-7

Single crystal X-ray diffraction study

The geometry of the synthesized complexes appeared in the form of a square planner by the single crystal analysis. Cu-O bond length in both the complexes is 180 A°. The bond distance between Cu-O(1) in complex-**7** & complex-**8** is 1.917(12) Å and 1.910(19) Å respectively.

[Cu(HL^{VII})$_2$] complex-7: Z= 2, α= 90°, β= 97.8400(10)°, γ= 90°, a = 8.4243(2)Å, b= 27.7723(4)Å, c= 7.01630(10)Å, **Monoclinic, *P*2$_1$/c** space group.

[Cu(HL^{VIII})$_2$] complex-8: Z= 2, α= 90°, β= 98.035(4)°, γ=90°, a = 7.2657(3)Å, b= 13.4359(4)Å, c= 18.2180(8)Å, **Monoclinic, *P*2$_1$/n** space group.

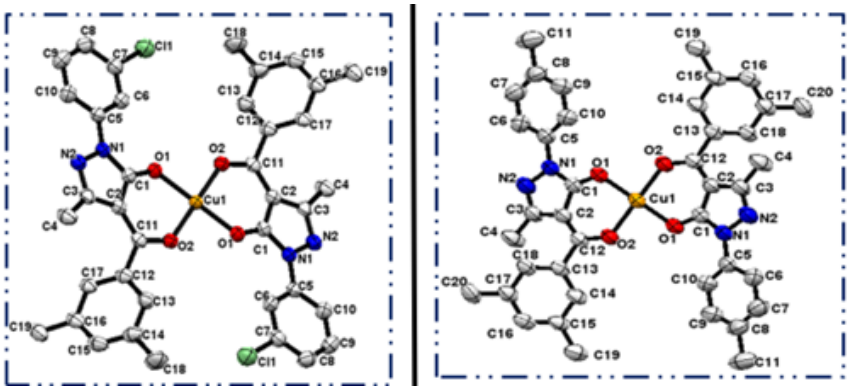

Fig.4b.4. ORTEP view of complex-7 and complex-8

DFT-based computational analysis & Hirshfeld surface area analysis

The geometries were computed using B3LYP/LANL2DZ levels for both complexes. The optimization energy -123.7430 keV and -100.8708 keV respectively were observed for complex-**7** & complex-**8.**

Electronic spectral analysis

Complex-7: π-π*(282 nm), n-π*(358 nm), d-d transition (705 nm), Molar absorbance (ε): 36.9 M^{-1} cm^{-1}. **Complex-8:** π-π*(278 nm), n-π*(375 nm), d-d transition (706 nm) Molar absorbance (ε): 36.9 M^{-1} cm^{-1}.

ESR & Electrochemical analysis

The value of $g_{\|}$ at LNT is found to be 2.3562, and $g_{\perp}$ is 2.0690. The value of g tensor is $g_{\|} > g_{\perp} >$ 2.0023 supports the Square Planner geometry. A geometric parameter G value is found to be 5.1623 by this formula $G = (g_{\|} - 2.0023)/(g_{\perp} - 2.0023)$.

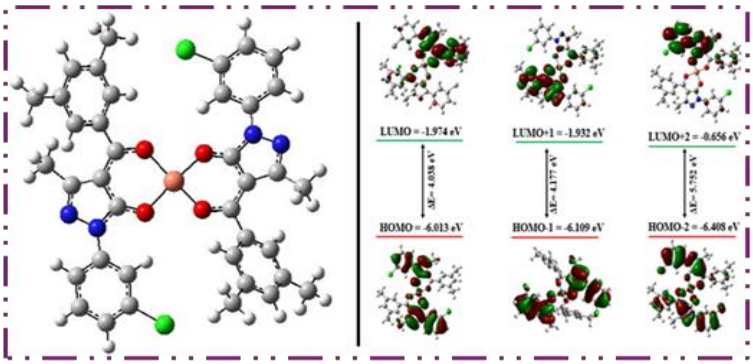

Fig.4b.5. DFT optimized geometry & HOMO-LUMO orbital of complex-7

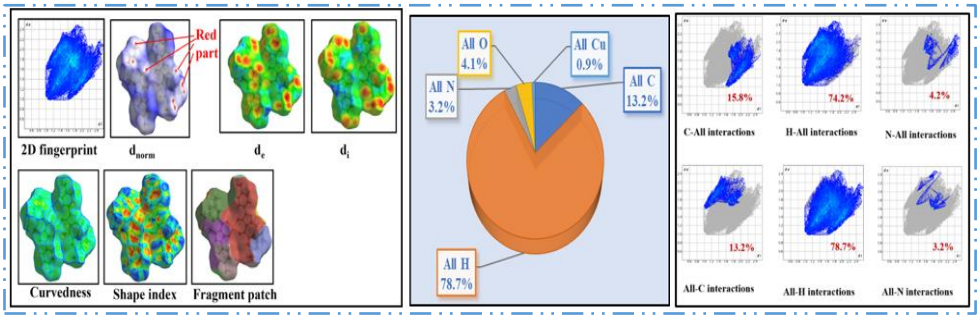

Fig.4b.6. Molecular hirshfeld diagram & 2d fingerprint plot of complex-8

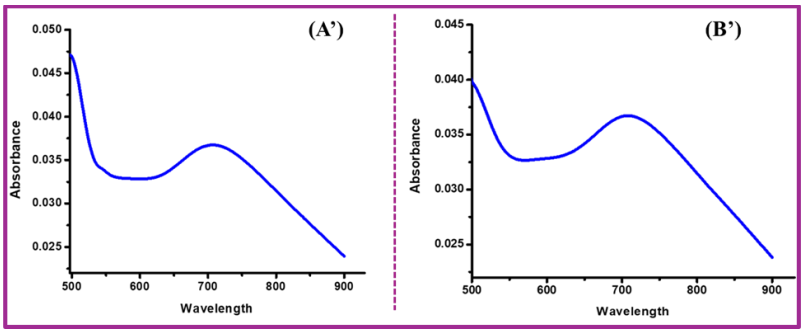

Fig.4b.7. d-d transition observed in complex-7 and complex-8

Spin density plot & NBO analysis

Natural Bond Orbital (NBO) analysis provided insights into hyperconjugative interactions and electron density transfer, showing Cu^{2+} with natural atomic charges of 1.1676 in complex-**8** and 1.1638 in complex-**7**. The electron configuration for copper in both complexes is [core] 3d

(9.13) 4s (0.34) 4p (0.36). Positive spin density is localized at the metal centre, while regions favouring the β spin state show negative density.

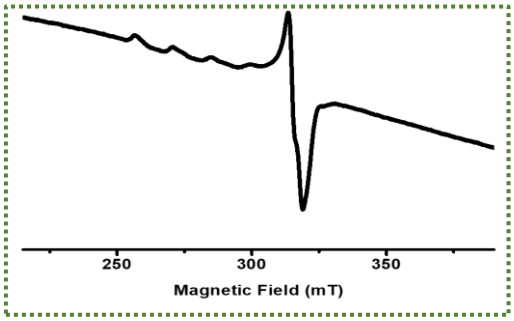

Fig.4b.8. X-band ESR spectra in the solution state at LNT

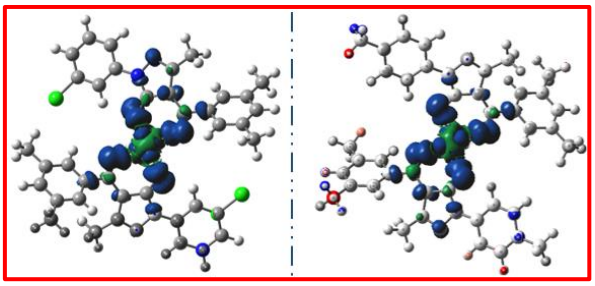

Fig.4b.9. Spin density plot of complex-7 & complex-8 respectively

4b.2.8. Cytotoxicity assay

MTT assay assessed the antiproliferative activity of complex-**8** on three cancer cell lines, with complex-**7** showing the highest efficacy against SH-SY5Y neuroblastoma cells, achieving a lower IC_{50} (3.9 µM) than cisplatin (44.9 µM). These results suggest that the copper complex is more effective than cisplatin

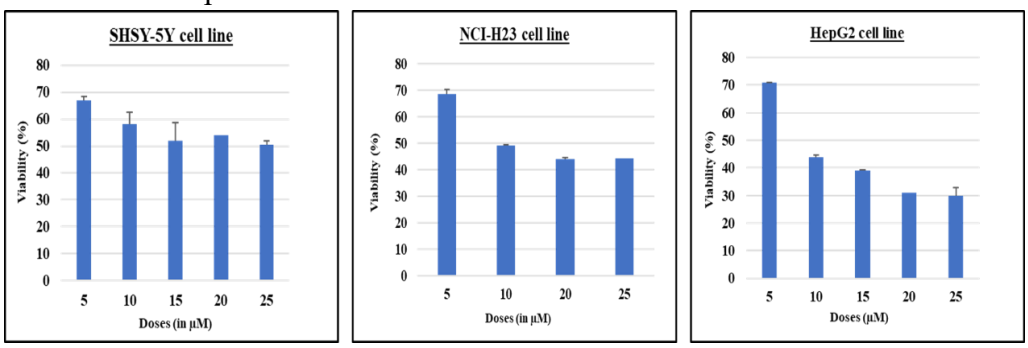

Fig.4b.10. Cell viability of NCI-H23, SH-SY5Y and HepG2 Cells exposed to indicated doses of complex-8

Conclusion

We successfully investigated new Cu(II) complexes with square planar geometry. A variety of analytical techniques were employed for the characterization. The computational study of the synthesized compounds was studied using the B3LYP/LanL2DZ basis set and the HOMO-LUMO energy gap was calculated. X-band ESR measurement at LNT was used to establish the complexes' magnetic properties. Lower IC_{50} value inspired the complex to compare with the well-known drug Cis platin against SH-SY5Y cancer cells.

CHAPTER 5

Chemical assessment of three Octahedral Ni(II) Complexes with heterocyclic Acylpyrazolone ligand: Crystal structure, DFT-NBO analysis, Hirshfeld and Magnetic study

Experimental work

Synthetic route of complexes 9, 10 & 11

Hot ethanolic solution of HL^{VIII} ligand, HL^{IV} ligand and HL^{VI} ligand and Nickel metal salt were taken in three different round-bottom flasks attached to a water condenser. The resulting mixture was refluxed for eight to ten hours at 80-90°C temperature in three separate round-bottom flasks. After Reflux, Pale green precipitates of all three synthesized Nickel complexes were produced. HL^{VIII}, HL^{IV}, and HL^{VI} all three ligands have already been reported in the previously published articles by our lab [23,11]. **HL^{VIII} ligand** (0.640g, 0.002 mol), **HL^{IV} ligand** (0.625g, 0.002 mol), **HL^{VI} ligand** (0.653g, 0.002 mol).

Complex-9: Pale bluish green crystal, yield: 81%, M.P:> 200°C, Molecular formula: $C_{44}H_{50}N_4NiO_6$, **M.W**: 789.58, **Elemental analysis**: C (Exp. 65.39%, Calc. 66.9%); H (Exp. 6.3%, Calc. 6.3%); N (Exp. 8.23%, Calc. 7.54%); Ni = 8.4% (Metal estimation- gravimetrically and volumetrically), **FTIR(KBr, cm^{-1}):** ν(C=O) of pyrazolone: (1596), ν(C=O) of benzoyl chloride: (1558), cyclic ν(C=N): (1486).

Complex-10: Pale green crystal, yield: 81%, M.P:> 200°C, Molecular formula: $C_{38}H_{36}Cl_2N_5NiO_6$, **M.W**: 788.32, **Elemental analysis**: C (Exp. 57.39%, Calc. 58.10%); H (Exp. 4.20%, Calc. 4.60%); N (Exp. 8.23%, Calc. 8.88%); Ni = 8.6% (Metal estimation-gravimetrically and volumetrically), **FTIR(KBr, cm^{-1}):** ν(C=O) of pyrazolone: (1613), ν(C=O) of benzoyl chloride: (1590), cyclic ν(C=N): (1457).

Complex-11: Pale yellow-green crystal, yield: 83%, M.P:> 200°C, Molecular formula: $C_{42}H_{46}Cl_2N_4NiO_6S_2$, **M.W**: 896.57, **Elemental analysis**: C (Exp. 55.92%, Calc.: 56.26%); H (Exp. 5.10%, Calc. 5.15%); N (Exp. 6.10%, Calc. 6.25%); Ni = 8.4% (Metal estimation gravimetrically and volumetrically), **FTIR(KBr, cm^{-1}):** ν(C=O) of pyrazolone: (1602), ν(C=O) of benzoyl chloride: (1540), cyclic ν(C=N): (1159).

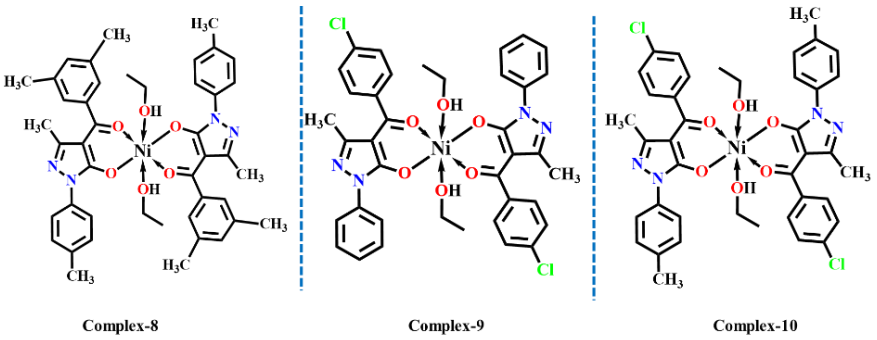

Fig.5.1. Structure of complexes 8, 9 and 10

Results and discussion

FTIR spectral studies and Thermogravimetric analysis

All the synthesized Nickel complexes are octahedral. TGA describes how the mass of a substance changes as a function of temperature. Thermal breakdown at temperatures between 100 and 550 °C serves as evidence of the remarkable thermal stability of the three synthesized Ni(II) complexes.

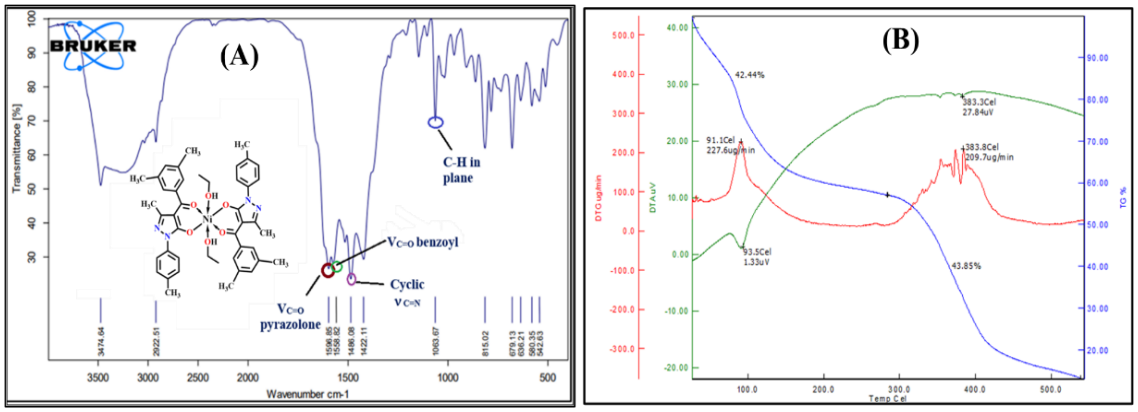

Fig.5.2. Complex-9: FTIR spectra of (A) FTIR spectrum and (B) TGA spectrum

Single crystal X-ray diffraction study and Powder XRD analysis

The structural analysis evidenced that the Ni centre is "octahedrally coordinated" from each six oxygen atoms in three complexes. Complex-**9** and complex-**10** crystallize in a 'Triclinic crystal system' with space group ***P*-1** while complex-**11** crystallizes in a 'Monoclinic crystal system' with space group ***P*2$_1$/n.**

In the XRD graph, a sharp band is observed with maxima 2θ = 5 to 25° range for complex-**11**. The simulated pattern matches well with the experimental pattern which confirms a similar geometry of the complexes. This also ensures the structure obtained from a single crystal represents the bulk of the complexes.

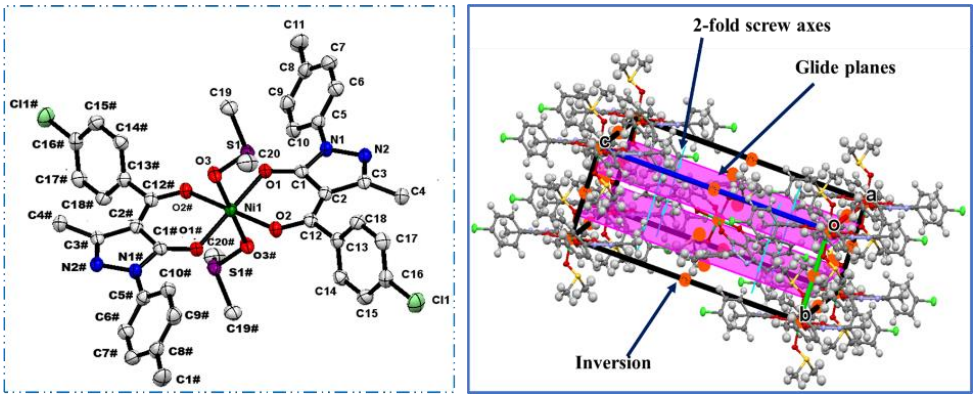

Fig.5.3. ORTEP view and symmetry elements of complex-11

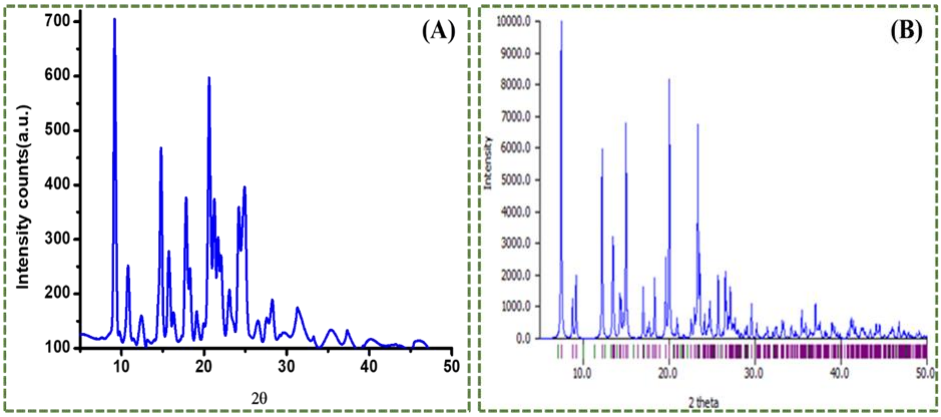

Fig.5.4. Experimental & Simulated powder XRD pattern of complex-11

Electronic spectral analysis and Magnetic study

Electronic transition(d-d spectra) of complex-**9** and complex-**11** were obtained in a 100% DMSO (1×10^{-3} M) solution up to 950 nm. While d-d bands of complex-**10** were obtained in 10^{-2} M concentration. A superconducting quantum interference (SQUID) device is used to study a material's magnetic characteristics at different magnetic fields and temperatures. Temperature-dependent magnetisation data at 500 Oe (0.05T) was obtained using SQUID. According to Curie–Weiss paramagnetism, Magnetic susceptibility is inversely proportional to temperature hence, by increasing temperature the susceptibility decreases.

Table 5.1. Band Assignments of all three Ni(II) complexes

	Complex-9	Complex-10	Complex-11
$3A_{2g}\rightarrow3T_{1g}(P)$	516 nm, (1.7 $M^{-1}cm^{-1}$)	502 nm, (2.0 $M^{-1}cm^{-1}$)	773 nm, (0.3 $M^{-1}cm^{-1}$)
$3A_{2g}\rightarrow3T_{1g}(F)$	652 nm, (4.0 $M^{-1}cm^{-1}$)	669 nm, (3.8 $M^{-1}cm^{-1}$)	752 nm, (1.7 $M^{-1}cm^{-1}$)
$3A_{2g}\rightarrow3T_{2g}$	773 nm, (0.3 $M^{-1}cm^{-1}$)	652 nm, (3.0 $M^{-1}cm^{-1}$)	770 nm, (0.5 $M^{-1}cm^{-1}$)

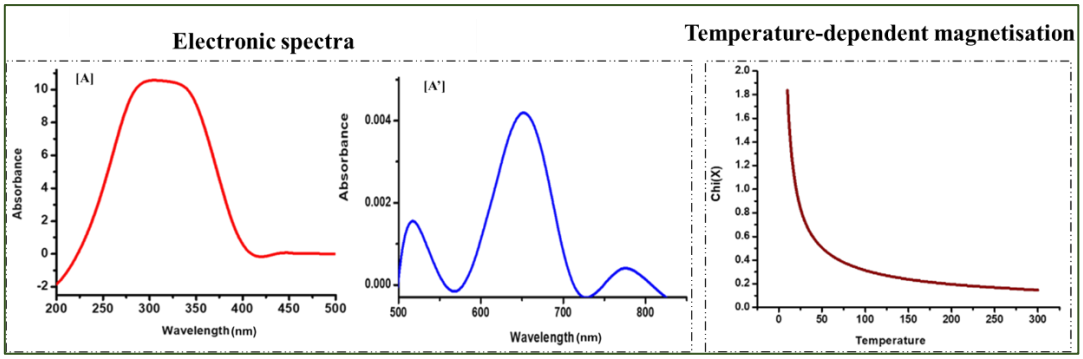

Fig.5.5. Electronic spectra and magnetization graph

DFT based computational analysis & Hirshfeld surface area analysis

The geometry of all three Ni(II) complexes was optimized via B3LYP/LANL2DZ level basis set using Gauss View 6.0 software. The optimization energy is -105.7622 keV, -64.0523 keV and -66.3350 keV of complex-**9,10 and 11**, respectively.

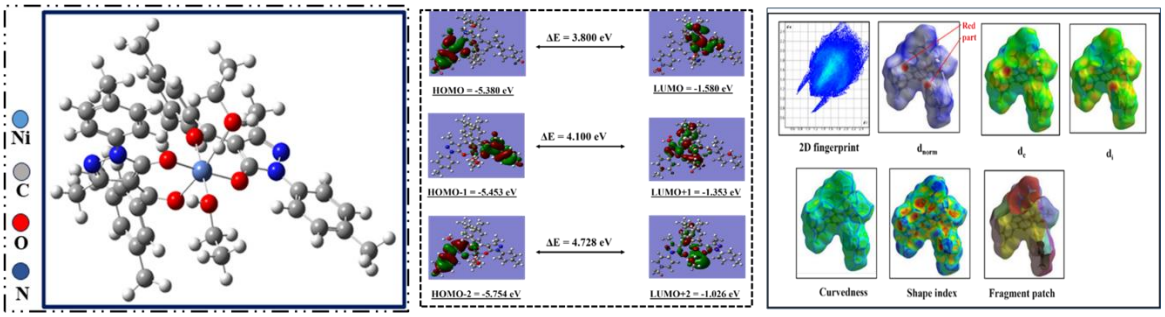

Fig.5.6. DFT optimized geometry, HOMO-LUMO orbitals and Hirshfeld diagram of complex-9

Conclusion

Acylpyrazolone-based three Ni(II) complexes were synthesized having Octahedral geometry. All three complexes were characterized using analytical methods. X-ray single-crystal diffraction data reveals that the ligand coupled to Ni(II) ions in all three complexes via O donor atoms. The magnetic study revealed the paramagnetic nature of the complexes. Multiple interactions have been identified through Hirshfeld surface analysis. DFT and HOMO-LUMO studies were conducted. The magnetic study revealed the paramagnetic nature of complexes.

References

[1] S. Ravichandran, R M Madhumitha Sri, M. Mehraj, C. Sowmya, The importance of transition metals as a drug, Int. J. Clin. Biochem. Res. 9 (2022) 1–3. https://doi.org/10.18231/j.ijcbr.2022.001.

[2] A. Wang, W. Wang, Superabsorbent Materials, Kirk-Othmer Encycl. Chem. Technol. 2009. https://doi.org/10.1002/0471238961.supewang.a01.

[3] F.K. Keter, J. Darkwa, Perspective: The potential of pyrazole-based compounds in medicine, BioMetals. 25 (2012) 9–21. https://doi.org/10.1007/s10534-011-9496-4.

[4] L. Knorr, A. Blank, Einwirkung substituirter Acetessigester auf Phenylhydrazin, Berichte Der Dtsch. Chem. Gesellschaft. 17 (1884) 2049–2052. https://doi.org/10.1002/cber.18840170299.

[5] B.S. Jensen, H. Meier, K. Lundquist, S. Refn, The Synthesis of 1-Phenyl-3-methyl-4-acyl-pyrazolones-5., Acta Chem. Scand. 13 (1959) 1668–1670. https://doi.org/10.3891/acta.chem.scand.13-1668.

[6] O.G. Idemudia, A.P. Sadimenko, E.C. Hosten, Metal complexes of new bioactive pyrazolone phenylhydrazones; crystal structure of 4-acetyl-3-methyl-1-phenyl-2-pyrazoline-5-one phenylhydrazone ampp-ph, Int. J. Mol. Sci. 17 (2016). https://doi.org/10.3390/ijms17050687.

[7] F. Marchetti, C. Pettinari, R. Pettinari, Acylpyrazolone ligands: Synthesis, structures, metal coordination chemistry and applications, Coord. Chem. Rev. 249 (2005) 2909–2945. https://doi.org/10.1016/j.ccr.2005.03.013.

[8] F. Marchetti, C. Pettinari, C. Di Nicola, A. Tombesi, R. Pettinari, Coordination chemistry of pyrazolone-based ligands and applications of their metal complexes, Coord. Chem. Rev. 401 (2019) 213069. https://doi.org/10.1016/j.ccr.2019.213069.

[9] E. Bagdatli, F. Yildirim, G. Ulucay, U. Sayin, Novel Copper (II) and palladium(II) complexes with 4-aroyl-5-pyrazolone ligands: Synthesis and characterization, J. Organomet. Chem. 896 (2019) 38–50. https://doi.org/10.1016/j.jorganchem.2019.05.026.

[10] S.P.C. Cole, Rapid chemosensitivity testing of human lung tumor cells using the MTT assay, Cancer Chemother. Pharmacol. 17 (1986) 259–263. https://doi.org/10.1007/BF00256695.

[11] I.U. Shaikh, Synthesis , Characterization and Studies on d^{10} Metal Complexes derived from Acyl Pyrazolones, (2020).

[12] M. Travadi, R.N. Jadeja, R.J. Butcher, M.S. Shekhawat, Neodymium based acylpyrazolone complexes: Synthesis and physicochemical characterizations, Inorganica Chim. Acta. 559 (2024) 121766. https://doi.org/https://doi.org/10.1016/j.ica.2023.121766.

[13] M. Travadi, R.N. Jadeja, R.J. Butcher, Uranyl (VI) Mixed-ligand complex synthesis and characterization using 4-acylhydrazone-5-pyrazolone and 4-acylpyrazolone : Covalency , crystal assay , DFT study and Hirshfeld analysis, J. Mol. Struct. 1281 (2023). https://doi.org/10.1016/j.molstruc.2023.135137.

[14] G. Vala, A.A. Puranik, R.N. Jadeja, D. Choquesillo-Lazarte, Solvent Free, Selective Oxidation of Styrene Catalyzed by Cobalt Acylpyrazolone Supported onto Neutral Alumina: Synthesis and Spectral Characterization, ChemistrySelect. 9 (2024). https://doi.org/10.1002/slct.202304086.

[15] P.R. Spackman, M.J. Turner, J.J. McKinnon, S.K. Wolff, D.J. Grimwood, D. Jayatilaka, M.A. Spackman, CrystalExplorer: A program for Hirshfeld surface analysis, visualization and quantitative analysis of molecular crystals, J. Appl. Crystallogr. 54 (2021) 1006–1011. https://doi.org/10.1107/S1600576721002910.

[16] G.M. Sheldrick, Crystal structure refinement with SHELXL, Acta Crystallogr. Sect. C Struct. Chem. 71 (2015) 3–8. https://doi.org/10.1107/S2053229614024218.

[17] S. Roy, P. Mitra, A.K. Patra, Cu(II) complexes with square pyramidal (N2S)CuCl2 chromophore: Jahn-Teller distortion and subsequent effect on spectral and structural properties, Inorganica Chim. Acta. 370 (2011) 247–253. https://doi.org/10.1016/j.ica.2011.01.068.

[18] A. Abayneh, T. Gebretsadik, S. Tadesse, M. Thomas, Synthesis, Spectroscopic, Structural Characterization, Conductivity and Electrochemical Studies of a Schiff Base Ligand and Its Copper Complexes, Adv. Chem. Eng. Sci. 08 (2018) 241–254. https://doi.org/10.4236/aces.2018.84017.

[19] S. Parihar, S. Pathan, R.N. Jadeja, A. Patel, V.K. Gupta, Synthesis and Crystal Structure of an Oxovanadium(IV) Complex with a Pyrazolone Ligand and Its Use as a Heterogeneous Catalyst for the Oxidation of Styrene under Mild Conditions, Inorg. Chem. 51 (2012) 1152–1161. https://doi.org/10.1021/ic202396q.

[20] DR. S. VALARSELVAN, Electronic Spectra of Transition metal complexes Spectroscopic ground states , spectral terms , R-S coupling and J-J couplings- term symbol – selection rules — microstates — Pigeon hole diagram for p2 and d2 configuration . Orgel and Tanabe – sugano diagr, n.d.

[21] A.V.P. Bobadilla, J. Arévalo, E. Sarró, H.M. Byrne, P.K. Maini, T. Carraro, S. Balocco, A. Meseguer, T. Alarcón, In vitro cell migration quantification method for scratch assays, J. R. Soc. Interface. 16 (2019). https://doi.org/10.1098/rsif.2018.0709.

[22] P.N. Tawakoli, A. Al-Ahmad, W. Hoth-Hannig, M. Hannig, C. Hannig, Comparison of different live/dead stainings for detection and quantification of adherent microorganisms in the initial oral biofilm, Clin. Oral Investig. 17 (2013) 841–850. https://doi.org/10.1007/s00784-012-0792-3.

[23] M. Travadi, R.N. Jadeja, R.J. Butcher, M.S. Shekhawat, Neodymium based acylpyrazolone complexes: Synthesis and physicochemical characterizations, Inorganica Chim. Acta. 559 (2024) 121766. https://doi.org/https://doi.org/10.1016/j.ica.2023.121766.

Research publications

1. S. Barad, K. Chaudhari, R.N. Jadeja, H. Roy, D. Choquesillo-Lazarte, Square pyramidal Cu(II) acylpyrazolone complex: Synthesis, characterization, crystal structure, DFT and Hirshfeld analysis, in-vitro anti-cancer evaluation, J. Mol. Struct. 1294 (2023) 136345. https://doi.org/10.1016/j.molstruc.2023.136345.

2. S. Barad, K. Chaudhari, H. Roy, R.J. Butcher, R.N. Jadeja, Acylpyrazolone based square pyramidal Cu(II) complexes: Synthesis, structural characterization, DFT and antiproliferative properties, Inorganica Chim. Acta. 559 (2024) 121794. https://doi.org/10.1016/j.ica.2023.121794.

3. S. Barad, K. Chaudhari, R.N. Jadeja, H. Roy, R.J. Butcher, Cytotoxicity assay and gene expression studies of acylpyrazolone-based square planar Cu(II) complexes: synthesis, characterization and computations, J. Coord. Chem. 76 (2023) 1955–1983. https://doi.org/10.1080/00958972.2023.2289004.

4. S. V. Barad, S. Saurabhb, D. Choquesillo-Lazarte, R.N. Jadeja, Chemical assessment of three octahedral Ni(II) complexes with heterocyclic acylpyrazolone ligand: Crystalstructure, DFT-NBO analysis, Hirshfeld and Magnetic study J. Mol. Struct. 1321 (2025) 140213. https://doi.org/10.1016/j.molstruc.2024.140213.

5. S.V. Barad, R.N. Jadeja, R.J. Butcher, Crystal structure, DFT and Hirshfeld surface analysis of acylpyrazolone based square pyramidal Copper(II) complex: *In-vitro* anticancer activity, Inorganica Chim. Acta (Under review, MS no. ICA-D-24-01168).

6. S.V. Barad, R.N. Jadeja, R.J. Butcher, Two New Square Planar Cu(II) complexesderived from a heterocyclic Pyrazolone ligand: Synthesis, *in vitro* anticancer activity, DFT and Hirshfeld analysis (Communicated).